Remote Sensing of Environment 182 (2016) 227–251

Contents lists available at ScienceDirect

Remote Sensing of Environment

journal homepage: www.elsevier.com/locate/rse

Global snow cover estimation with Microwave Brightness Temperature measurements and one-class *in situ* observations

Xiaocong Xu, Xiaoping Liu *, Xia Li *, Qinchuan Xin, Yimin Chen, Qian Shi, Bin Ai

School of Geography and Planning and Guangdong Key Laboratory for Urbanization and Geo-simulation, Sun Yat-sen University, Guangzhou 510275, PR China

ARTICLE INFO

Article history:
Received 7 September 2015
Received in revised form 16 April 2016
Accepted 15 May 2016
Available online 31 May 2016

Keywords:
Global snow cover
One-class classification
Presence and Background Learning (PBL) algorithm
Microwave Brightness Temperature (BT)

ABSTRACT

Brightness temperature (BT), which is remotely sensed by the space-borne microwave radiometer, is widely used in snow cover monitoring for its long time series imaging capabilities in all-weather conditions. Traditional linear fitting and stand-alone methods are usually uncertain with respect to the spatial distribution and temporal variation of derived snow cover, as they rarely consider local conditions and scene characteristics but fit the model with static empirical coefficients. In this paper, a novel method utilizing daily ground *in situ* observations is proposed and evaluated, with the purpose for accurate estimation of long-term daily snow cover. To solve the challenge that ground snow-free records are insufficient, a one-class classifier, namely the Presence and Background Learning (PBL) algorithm, is employed to identify daily global snow cover. Benefiting from daily ground *in situ* observations on a global scale, the proposed method is temporally and spatially dynamic such that estimation errors are globally independent during the entire study period. The proposed method is applied to the estimation of global daily snow cover from 1987 to 2010; the results are validated by ground *in situ* observations and compared with available optical-based and microwave-based snow cover products. Promising accuracy and model stability are achieved in daily, monthly and yearly validations as compared against ground observations (global omission error <0.13, overall accuracy >0.82 in China region, and keep stable in monthly and yearly averages). The comparison against the MODIS daily snow cover product (MOD10C1) shows good agreement under cloud-free conditions (Cohen's kappa = 0.715). The comparison against the NOAA daily Interactive Multisensor Snow and Ice Mapping System (IMS) dataset suggests promising agreement in the Northern Hemisphere. Another comparison against the AMSR-E daily SWE dataset (AE_DySno) demonstrates the efficiency of the proposed method regarding to the overestimation problem in thin snow cover region.

1. Introduction

The seasonal snow cover of the globe, especially in the Northern Hemisphere, has a significant impact on climate, water cycles and biogeochemical cycling, as the surface albedo of the northern areas in winter season is mainly controlled by snow covered area. As snow cover can affect climate dynamics (Cohen & Entekhabi, 1999), the capacity for the accurate estimation of global snow cover and the volumetric storage of water in snowpack limits our ability to monitor climate change and test climate model simulations. Traditional snow cover monitoring was mainly based on isolated ground observations from meteorological stations. However, sparse point observation networks can hardly provide the overall picture on regional and global scales due to their low spatial densities or even complete absence in inaccessible regions (Walker, Derksen, & Goodison, 2005). Remote sensing has been used to monitor continental-scale seasonal snow cover for more than two decades (Allan & David, 1999). Various studies have shown that snow cover can be detected using both optical sensors (Allen, Durkee, & Wash, 1990; Hall, Riggs, Salomonson, Digirolamo, & Bayr, 2002; Hall, Riggs, & Salomonson, 1995) and space-borne positive microwave radiometers (Klein & Barnett, 2003; Walker & Goodison, 1993).

Since the 1980s, a number of algorithms have been developed for snow cover monitoring using optical sensors, such as the multi-spectral thresholds classification method (Allen et al., 1990; Romanov, Gutman, & Csiszar, 2000), linear spectral unmixing for subpixel snow cover mapping (Romanov, Tarpley, Gutman, & Carroll, 2003; Rosenthal & Dozier, 1996), and the Normalized Difference Snow Index (NDSI) algorithm (Hall et al., 2002; Hall et al., 1995). However, snow cover observations through optical sensors are sensitive to local weather conditions, especially when cloud cover and rainfall are present. Moreover, sunlight is required to receive the reflected signal from snowpack to the optical sensors. Thus it is difficult to find consecutive daily images that are cloud-free or have low cloud cover percentage. Obscuration by cloud cover and inaccessibility in dark regions greatly limit the applicability of optical-based snow cover products in regional and global applications. (Klein & Barnett, 2003; Wang, Xie, Liang, & Huang, 2009).

* Corresponding authors.

http://dx.doi.org/10.1016/j.rse.2016.05.010
0034-4257/

Passive microwave observation from space-borne radiometers is another data source for the retrieval of global/regional snow cover or snow water equivalent (SWE) because of its wide swath, all-weather imaging capabilities, day and night time capability, multi-frequency response to the presence of snow pack, and a long archive history dating back to 1978. Progress in retrieving snow cover or SWE has been made since the launch of the Scanning Multi-Channel Microwave Radiometer (SSMR) in 1978 and the Special Sensor Microwave Imager (SSM/I) in 1987. Although these two microwave sensors are not designed for snow detection, they have been found to be effective in detecting snow cover and SWE (Chang, Foster, Hall, Rango, & Hartline, 1982; Chang, Foster, & Hall, 1987; Pulliainen, 2006; Walker & Goodison, 1993). The Advanced Microwave Scanning Radiometer - EOS (AMSR-E), which was launched in 2002 and stopped in 2011, and its successor the Advanced Microwave Scanning Radiometer 2 (AMSR2), which was launched in 2012, provide other microwave data sources with relatively higher spatial resolution for the mapping of the snow cover and SWE (Kelly, Chang, Tsang, & Foster, 2003; Tedesco, Kelly, Foster, & Chang, 2004).

The detection of snow cover and SWE from microwave observations is based on the fact that the presence of snowpack on land surface causes a difference of microwave scattering and can be detected by space-borne instruments. On snow covered surfaces, brightness temperature (BT), a measure of microwave emission, tends to decrease with increasing snow depth since larger number of snow crystals scatter more microwave signal. Traditional snow cover retrieval methods model the snow depth (or SWE) as a function of the difference between of multi-frequency BTs. The algorithm proposed by Chang et al. (Chang et al., 1987) is a typical example. Based on this work, a number of studies were carried out to improve the accuracy and stability of snow cover and snow depth (or SWE) retrievals by taking into account the effects of grain size, snow density and vegetation canopy, *etc.* (Foster, Chang, & Hall, 1997; Kelly, Chang, Foster, & Hall, 2001; Pulliainen, Grandell, & Hallikainen, 1999).

Although previous studies achieved acceptable accuracies for some regions and seasons, the snow cover and SWE estimates based on microwave data are found to be spatial and temporal bias (Pulliainen, 2006). Moreover, most microwave snow cover retrievals are reported to underestimate the snow cover in regions of low elevation and overestimate the snow cover in mountainous areas (Foster et al., 1997; Koenig & Forster, 2004). These problems probably result from insufficient considerations of spatial and temporal heterogeneity of snowpack and land cover in these stand-alone algorithms. Besides, the empirical regression coefficients in these models are often calibrated by insufficient ground observations of snow information, *i.e.*, dozens of sparse observations in short time period. The accuracy of such snow cover retrievals is closely dependent on local conditions and scene characteristics, crippling the applicability of these models for producing a promising snow cover datasets for a long-term period.

One potential solution to overcome these challenges is to integrate a global long-term series of ground snow observations with microwave-based snow cover modeling. The Global Surface Summary of Day (GSOD) dataset, which is provided by the National Climatic Data Center (NCDC), is a potential data source to provide sufficient ground snow cover observations. The GSOD dataset is contributed by more than 29,000 meteorological stations across the globe (see Fig. 3). It provides various meteorological elements, including snow depth information, dating back to 1929. Currently, approximately 9000 stations are functional in acquiring ground snow cover information. However, snow-free records in the GSOD dataset are mixed with missing observation records, *i.e.*, we cannot identify whether a record is snow-free or an unreported snow presence. Without observed snow-free records, traditional binary classifier-based methods of snow cover discrimination (*e.g.*, support vector machine, maximum likelihood estimation) are not applicable to the modeling of snow cover over selected attributes.

The purpose of this study is to develop and test a one-class method, namely the Presence and Background Learning (PBL) algorithm, to estimate the global snow cover even though there are no reliable reports of snow-free on the ground. By integrating long-term daily ground snow cover information with space-borne microwave BT measurements, the proposed method is different from previous static stand-alone algorithms, but expected to be temporally and spatially dynamic. The accuracy and variation of our model estimation are independent from local conditions and scene characteristics such that the method is applicable for accurate long-term snow cover estimation under all-weather conditions. The proposed method involves two steps. First, space-borne microwave BT measurements and massive one-class ground *in situ* snow cover observations are combined to train the PBL model to estimate the probability of snow cover presence. Second, an appropriate threshold is automatically selected to segment the estimated probability into binary class: snow-free and snow cover. Since the model utilized ground observations and microwave measurements on a daily basis, the proposed model should be temporally and spatially dynamic such that estimation errors are independent from local conditions and scene characteristics.

2. Datasets used in the study

2.1. The SSM/I Brightness Temperature (BT) dataset

The SSM/I brightness temperature dataset (Armstrong, Knowles, Brodzik, & Hardman, 1994) used in this study is collected from the Special Sensor Microwave/Imager (SSM/I) sensors, which are boarded on the Defense Meteorological Satellite Program (DMSP) series satellites. The SSM/I sensor is a multi-frequency (19-, 22-, 37- and 85-GHz) microwave radiometric system. Both vertical and horizontal polarization are measured for all but not 22-GHz, for which only the vertical polarization is measured. The foot print varies with channel energy, ranging from 69×43 km^2 at 19-GHz to 15×13 km^2 at 85-GHz (Hollinger, 1991). The SSM/I BT data are gridded into NSIDC Equal-Area Scalable Earth grids (EASE-Grids) for each day and projected into the cylindrical equal-area projection (Armstrong & Brodzik, 1995). The spatial resolution is 25×25 km^2 for all channels, and the 85-GHz channel is additionally available at 12.5×12.5 km resolution.

2.2. The Global Surface Summary of Day (GSOD) product

The Global Surface Summary of Day (GSOD) product is provided by the National Climatic Data Center (NCDC, https://data.noaa.gov/dataset/global-surface-summary-of-the-day-gsod), and is based on data exchanged under the World Meteorological Organization (WMO) World Weather Watch Program according to WMO Resolution 40 (Cg-XII). It is comprised of a dozen daily averaged weather parameters computed from global hourly station data. Snow depth is one of the 14 daily weather elements included in this dataset. The dataset is available since 1929, with around 29,000 meteorological stations covering over the globe. Currently more than 9000 stations are typically functional. The GSOD data provides snow depth information in inches to tenths; however, most stations do not report 0 values on days with no snow cover on the ground. Instead, the value of 999.9 will be archived in the dataset, which is the same value to denote a missing observation. Thus we cannot determine the occurrence of snow if a particular station reports a 999.9 value. This becomes the challenge of using the GSOD dataset as most records contain only presence data (observed snow cover) but lacking absence information (observed snow absence). Traditional two-class classifiers, such as support vector machine, maximum likelihood estimation, are not applicable due to the deficiency of absence data. The one-class PBL model investigated in this study is an attempt to overcome this challenge.

Table 1
Linear combinations of BTs and their corresponding materials considered in this study.

Linear combinations	Corresponding materials
T19V-T37V	Scattering signature, frozen surface
T22V-T85V	Scattering signature, precipitation cloud
T19V-T19H	Cold desert, shadow snow, melting snow
37V-T37H	Melting snow
T37V-T85V	Cold desert

2.3. The China Meteorological Station Observation (CMSO) dataset

For various reasons, stations located in China are all labeled as 999.9 in the snow depth field throughout the entire study period. Thus we used the China Meteorological Station Observation (CMSO, acquired from the China Meteorological Data Sharing Service System http://cdc.nmic.cn/home.do) dataset as Supplementary material to fill the missing data in the China region. The dataset contains 747 stations scattered throughout China, with around 300 stations typically functional on snow depth observation. Different from the GSOD dataset, the observed absence of snow cover is archived in the CMSO dataset, which means both the presence and absence data are available. However, it is not appropriate to estimate global snow cover by training a model from the observed absence data only available in China region. Thus the observed absence data in this dataset is only used for validation.

3. Theoretical basis for snow cover retrieval

The ability to identify snow cover from the observation of microwave electromagnetic spectrum is based on the fact that a difference of microwave scattering can be observed when snowpack is present in the ground surface. Microwave BT tends to decrease with increasing snow depth and snow density since the greater number of snow crystals provides increased scattering of the microwave signal. In this paper, we use the difference between BTs at low (19 GHz) and high (37 GHz) frequency to detect the source of scattering signals. A positive difference is inherent to a scattering surface and might possibly be attributed to snowpack (Chang et al., 1982). A greater observed difference implies stronger scattering signal, and a greater snow volume is assumed to be present. However, the observed scattering signals might also be caused by other surface

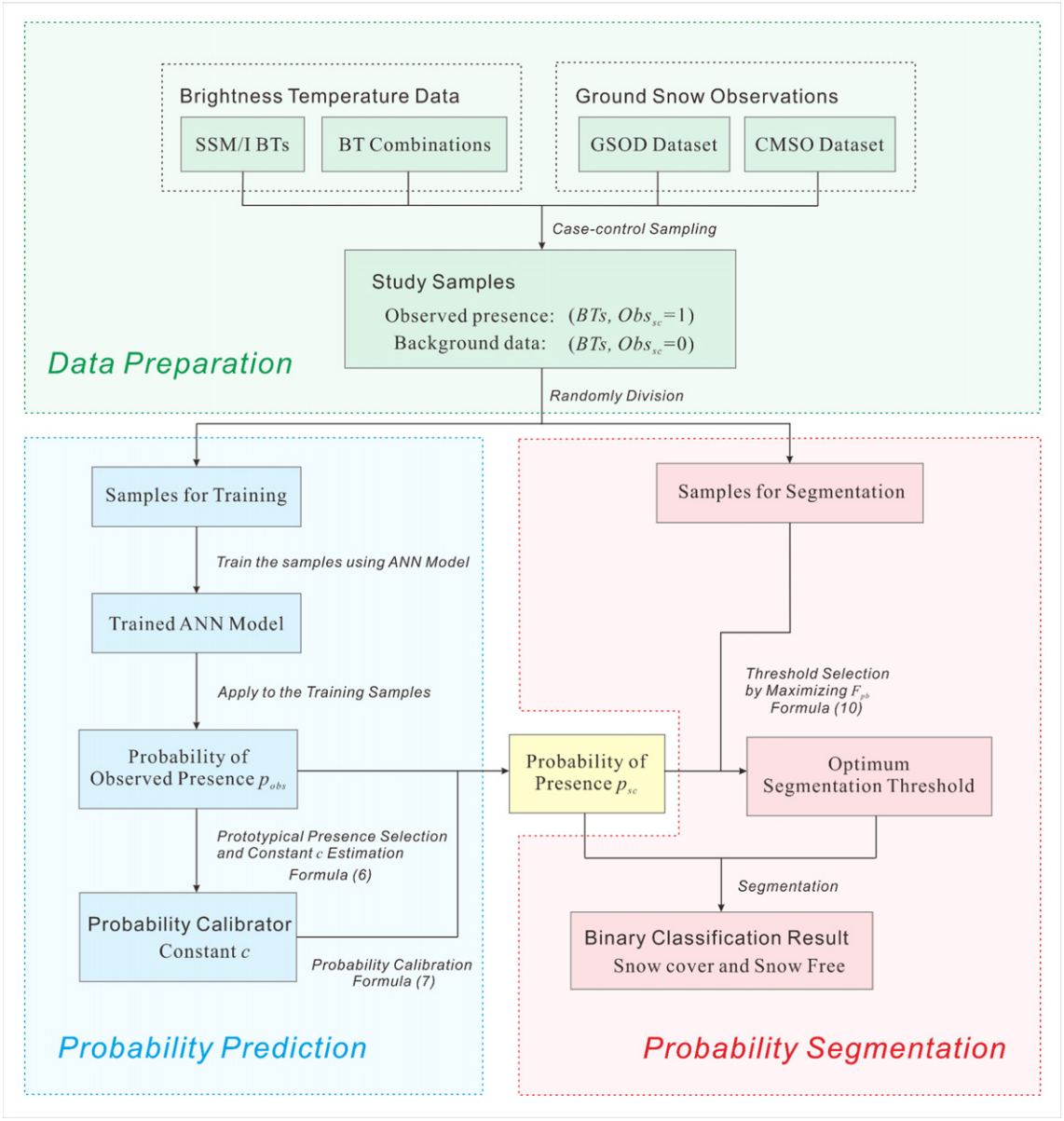

Fig. 1. A brief flow chart of the implementation of the PBL algorithm.

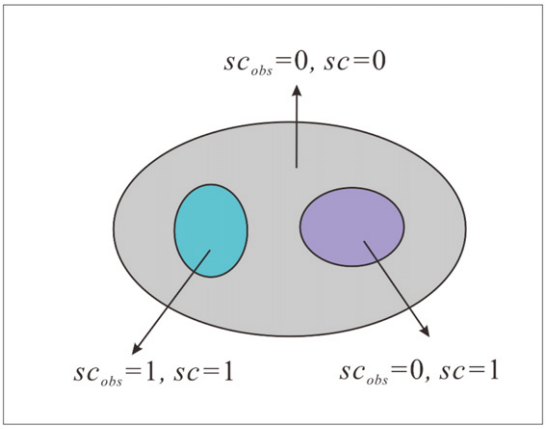

Fig. 2. Schematic drawing of the affiliation among different samples in the PBL model.

materials such as cold deserts and frozen ground. In addition, precipitating clouds can produce scattering signals in high frequency measurements. Previous researches used the liner combination of BTs to eliminate some of these interferential surface materials. For example, Grody (Grody, 1991; Grody & Basist, 1996) used an empirical combination $T19V-T37V\leq 2K \cap T22V-T85V\leq 6K$ to remove the frozen ground. Yu (Yu et al., 2011) used the condition $T18V-T18H\geq 18K \cap T36V-T85V\leq 10K$ to detect cold desert area. Walker and Goodison (Walker & Goodison, 1993) combined $T36V - T36H > 10K$and surface temperature > 270 K to identify the wet snow.

In this study we consider the following linear combinations listed in Table 1. Unlike previous studies, we did not use empirical thresholds to manually remove these interferential materials. Instead, we include them in our proposed model in which the BT linear combinations and surface materials are trained automatically. In addition, BTs at 19–37- and 85-GHz at available polarizations are also used to train the model, with the purpose to find out as many underlying attributes as possible for distinguishing snow cover from other interferential materials. As long as ground observations (should be "snow free") in interferential regions are utilized in the model training process, the trained algorithm based on Artificial Neural Network (ANN) will automatically learn the difference between the snowpack and the interferential surface materials, and label these interferential surfaces as "snow free". The advantage of such way to eliminate precipitating clouds and frozen soil/rocks is that we can avoid human interference, and let the model train and predict the snow cover pattern automatically and adaptively. By using the proposed method, the estimated probability of snow cover in areas of precipitating clouds and frozen soil/rocks would be relatively small. Moreover, the model is designed to be calibrated by daily ground observations, by which these interference surfaces will not be classified as snow cover, and therefore the estimated pattern of snow cover needs no post-eliminations.

4. One-class snow cover retrieval model

4.1. Estimation of snow cover probability based on PBL

The Presence and Background Learning algorithm (Li, Guo, & Elkan, 2011) is an effective tool in ecological studies for estimating the probability of a species' occurrence at given environmental covariates. The major feature of PBL is that it can accurately predict and calibrate the probability of target's occurrence without negative samples in the training set. This characteristic of the PBL model enables us to identify the snow cover extent considering that the snow-free observation is not available in the GSOD dataset. The main purpose of this section is to model the probability of snow cover occurrence on selected attributes (microwave BTs and their linear combinations) using the PBL model. A brief flow chart is provided in Fig. 1 to describe the implementation of the algorithm, including data preparation, probability prediction, and segmentation.

Before the methodology description, a few definitions need to be clarified in our snow cover estimation. We denote the presence of snow cover as $sc = 1$ and the absence as $sc = 0$. However, samples in the GSOD dataset which record snow cover occurrence in stations are slightly different from $sc = 1$. A more appropriate definition for such samples is *observed presence*, denoted as $obs_{sc} = 1$. The observed presence samples $obs_{sc} = 1$ are a subset of all presence samples $sc = 1$ that are happened to be observed by the instruments. Moreover, records that are labeled as 999.9 in the GSOD dataset are defined as *background sample*, denoted as $obs_{sc} = 0$. Note that a background sample is either an unknown presence or an unknown absence. If $obs_{sc} = 1$, then we know for sure that $sc = 1$; however, if $obs_{sc} = 0$, we do not know whether $sc = 1$ or $sc = 0$. A schematic drawing of the affiliation among different samples is showed in Fig. 2:

Given the above definitions, the probability of snow cover occurrence can be expressed as a conditional probability:

$$p_{sc} = P(sc = 1|BTs). \tag{1}$$

The *BTs* in Eq. (1) denotes the attributes (brightness temperature and their linear combinations) considered in the modeling. Unfortunately, the probability p_{sc} cannot be directly derived from the current available dataset using traditional methods because of the deficiency of absence snow cover samples. However, by training a binary classifier using the observed presence data (BTs, $obs_{sc} = 1$) and the background data (BTs, $obs_{sc} = 0$), another model can be established to estimate the probability of *observed presence* of snow cover on a specific site:

$$p_{obs} = P(obs_{sc} = 1|BTs, \eta = 1). \tag{2}$$

Note that $\eta = 1$ denotes the presence-background scenario. The strategy of the PBL algorithm is to first model the probability of an observed presence p_{obs} and then adjust it into the desired one p_{sc} through a series of probability transformations. To achieve this, the sampling method in the PBL algorithm is slightly different from that of the traditional presence-absence scenario. The case-control sampling method is applied to randomly select the study samples: it is assumed that observed presences (BTs, $obs_{sc} = 1$) are randomly sampled from all presence records (BTs, $sc = 1$), and background data (BTs, $obs_{sc} = 0$) are randomly sampled separately from the entire study region Ω.

Let p_1 be the number of observed presence data samples (BTs, $obs_{sc} = 1$) in the training set. Moreover, we assume the background data samples (BTs, $obs_{sc} = 0$) in the training set contain p_2 presences $sc = 1$ and n_2 absences $sc = 0$, which are in proportion to their overall

Table 2
Confusion metrics from presence-absence data (left) and presence-background data (right).

		Reference			
		$sc = 1$	$sc = 0$	$sc_{obs} = 1$	$sc_{obs} = 0$
Prediction	$sc_{pre} = 1$	*TP* (true positive)	*FP* (false positive)	*TP′* (true positive)	*FP′* (false positive)
	$sc_{pre} = 0$	*FN* (false negative)	*TN* (true negative)	*FN′* (false negative)	*TN′* (true negative)

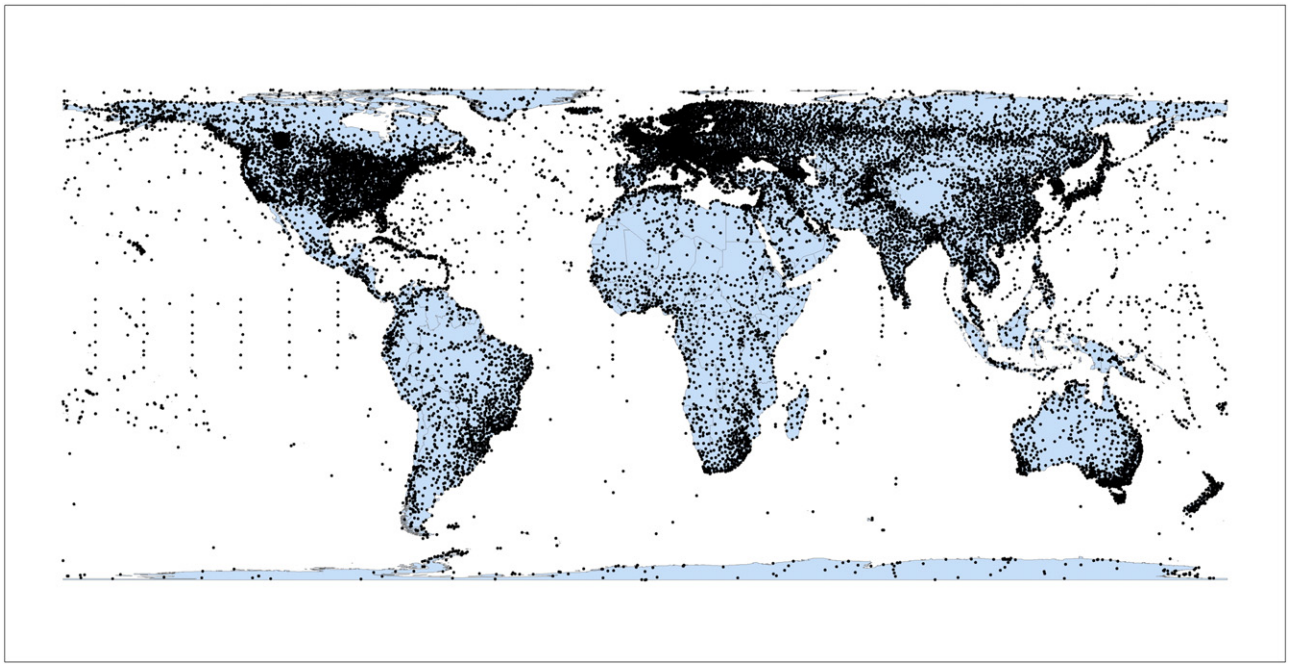

Fig. 3. Spatial distribution of the meteorological stations contributed to the GSOD dataset.

population prevalence in the entire study region. Because of the case-control sampling method, a connection between the presence of snow cover p_{sc} in Eq. (1) and the observed presence of snow cover p_{obs} in Eq. (2) can be built and expressed as (Li et al., 2011):

$$p_{sc} = \frac{p_2}{p_1} \times \frac{p_{obs}}{1 - p_{obs}}. \tag{3}$$

According to Eq. (3), the probability of the presence of snow cover p_{sc} is proportional to $p_{obs}/(1 - p_{obs})$, and the scale factor p_2/p_1 is the ratio of the number of presences among the background sample and the number of observed presence samples. In order to estimate p_2/p_1, we define a constant $c$as $c = p_1/(p_1 + p_2)$, and then we have $p_2/p_1 = (1 - c)/c$. Thus, if we can estimate this constant c, the probability of observed presence of snow cover p_{obs} can be adjusted into the probability of the presence of snow cover p_{sc}.

To estimate the constant c, the PBL model introduces another definition of *prototypical presence*. It means that, in the ecological studies, the habitat is maximally suitable for a specific species, so the species has a chance of 100% to survive in the corresponding habitat. In the context of snow cover estimation, we analogously assume that some stations in the study region have 100% estimated probability to be snow cover regarding a set of given BTs. These station observations are defined as *prototypical presence* of snow cover. Let O be a subset of samples that are located at stations of prototypical presence. Then we have

$$P(sc = 1|BTs) = 1 \quad BTs \in O. \tag{4}$$

According to the definition of conditional probability, it can be proved that

$$\begin{aligned} p_{obs} &= P(obs_{sc} = 1|BTs, \eta = 1) \\ &= \frac{p_1}{p_1 + p_2} \qquad\qquad BTs \in O \\ &= c \end{aligned} \tag{5}$$

The details of the derivation process in Eq. (5) can be found in the work of Li et al. (Li et al., 2011). Eq. (5) implies that, as to samples belonging to O, any predicted probabilities of the observed presence of snow cover p_{obs} can be used to estimate the constant c. In practice, a more reliable estimator of constant c is the average value of all samples belonging to O:

$$c = \frac{1}{n} \sum\nolimits_{BTs \in O} P(obs_{sc} = 1|BTs, \eta = 1) \tag{6}$$

where n is the population of O.

So far, we can build up a model to estimate the probability of snow cover p_{obs} indirectly from the presence and background data through 3 phases: Phase #1, a model is trained to estimate the probability of observed presence of snow cover from observed presence samples (BTs, $obs_{sc} = 1$) and background data (BTs, $obs_{sc} = 0$). Phase #2, a constant c is estimated according to Eq. (6) from the observations of prototypical presence stations in O. Phase #3, the trained model $p_{sc} = P(sc = 1|BTs)$ is adjusted into a desire model using the following equation:

$$p_{sc} = \frac{1 - c}{c} \times \frac{p_{obs}}{1 - p_{obs}}. \tag{7}$$

In phase #1, the training process can be implemented by traditional binary classifier (*e.g.* neural networks, logistic regression, generalized linear and additive models, and support vector machines). Studies have shown that artificial neural networks (ANN) are capable of estimating posterior probability and fit different types of models effectively (Richard & Lippmann, 1991). Thus we used a back-propagation (BP) neural network (Hecht-Nielsen, 1989) to model the probability of observed presence of snow cover for observed presence and background samples. In phase #2, estimating constant c needs to determine the prototypical presence sample set O beforehand. In practice, the top percentile of the estimated probability of observed presence $p_{obs} = P(obs_{sc} = 1|BTs, \eta = 1)$ in phase #1 are regarded as prototypical presence. For example, Li (Li et al., 2011) used the top 50% of the observed presences as prototypical presence modeling the probability of species occurrence. In our snow cover estimation model, we find that 50% percentile is reasonable in determining the prototypical presence sample set O. After phase #1 and phase #2, the desired probability p_{sc} can be estimated according to Eq. (7).

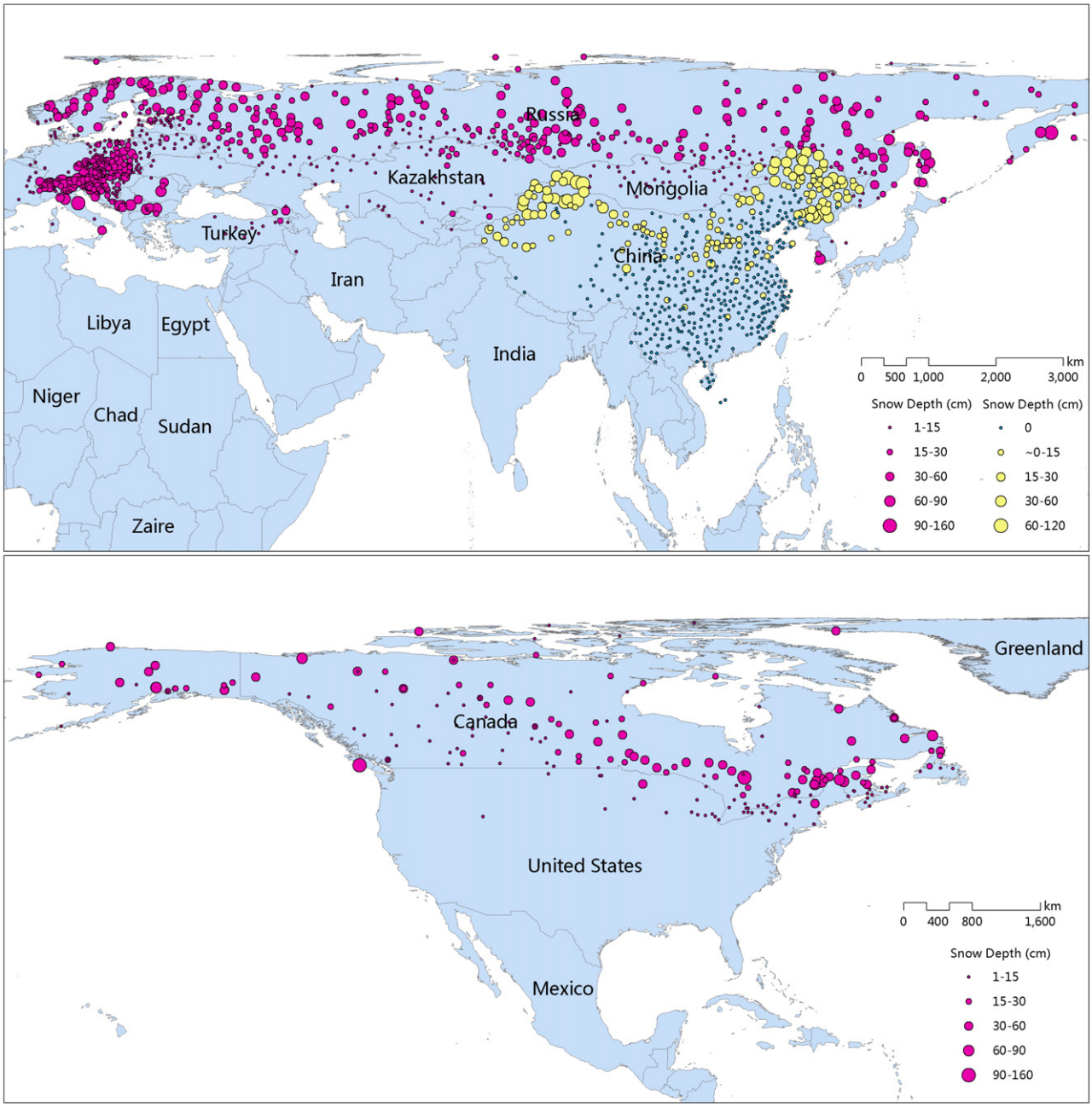

Fig. 4. Spatial distribution of stations with observations of snow cover presence on Jan. 6th, 2006, (up) Eurasia, (down) North America. Larger circle indicates deeper snow depth.

4.2. Probability segmentation using modified F-score

The original outputs of the PBL model is continuous probability of snow cover occurrence. It is necessary to select an appropriate threshold by which continuous probabilities will be classified into binary class: snow cover and snow-free. The objective of the threshold selection is to find a value that can maximize the classification accuracy over an independent validation dataset (Liu, Berry, Dawson, & Pearson, 2005).

Generally, classification results are compared against an independent validation set, and then a binary confusion matrix is created to cross-tabulate the classified and observed positive-negative labels (Table 2 left). Two types of errors can be estimated from the confusion matrix: commission and omission errors. The commission error indicates false positive (*FP*), the number of absence samples predicted as presences, whereas the omission error indicates false negative (*FN*), the number of presence samples predicted as absences. Combinations of commission and omission errors, such as the overall accuracy (Congalton, 1991), kappa coefficient (Cohen, 1960) and F-measure (Rijsbergen, 1979) have been shown to be effective in quantifying the accuracy of classification result. However, all of these metrics require both presence and absence data, by which the commission error and omission error can be estimated in advance. Thus the above-mentioned accuracy metrics are difficult to be applied to our one-class snow cover classification.

In order to modify the traditional accuracy metric and make it applicable for presence-background scenario, a new confusion matrix is created analogously to the original one, as shown in (Table 2 right). Based on this new confusion matrix, the modified expression of *F-measure* (Li & Guo, 2013), which is defined in Eq. (8), is applied for the assessment of snow cover estimation.

$$F_{cpb} = \frac{2 \times TP'}{TP' + FN' + c' \times FP'} \tag{8}$$

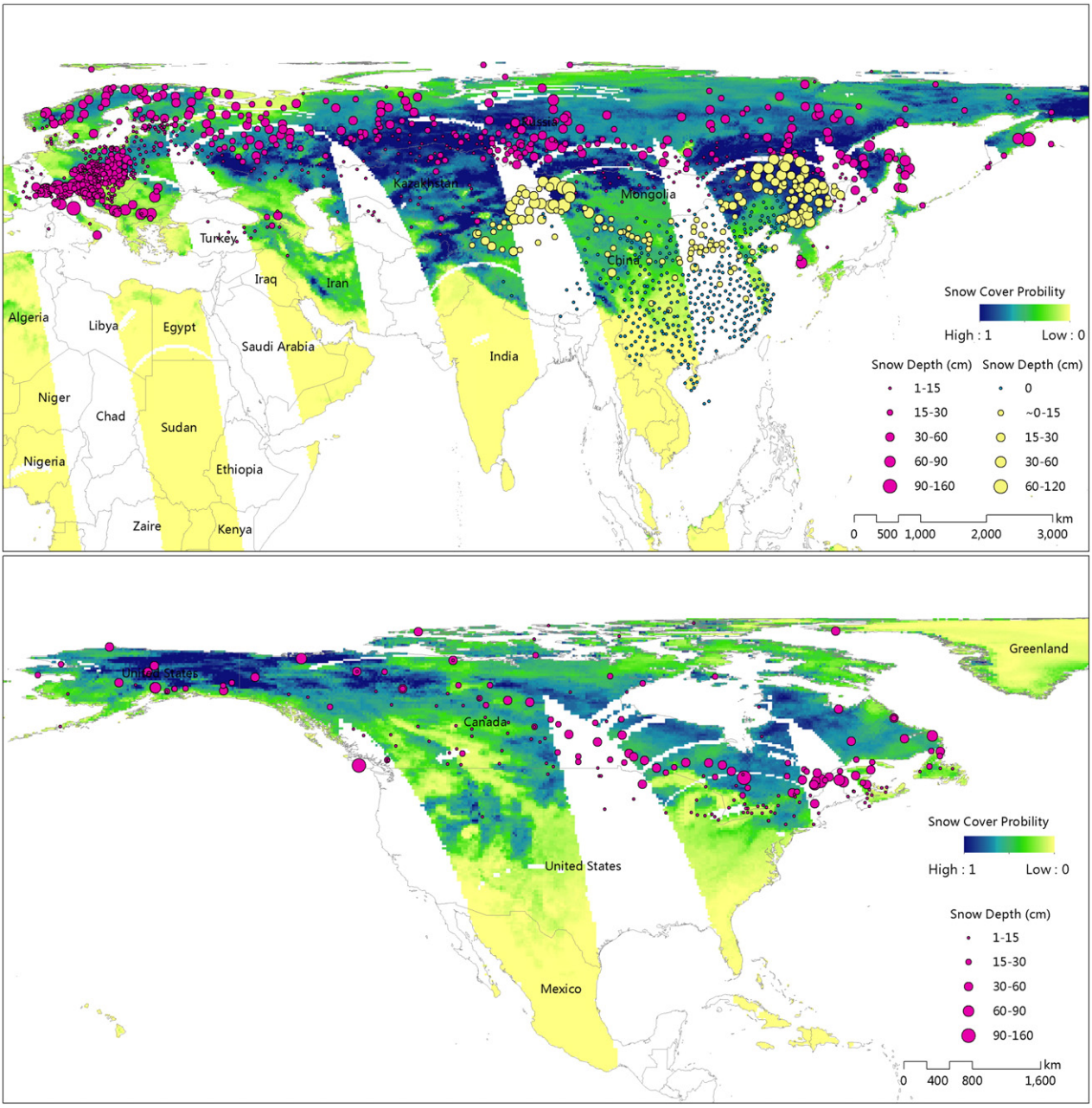

Fig. 5. Estimated probability of snow cover occurrence on Jan. 6th 2006, overlapped with *in situ* ground observations from one-class GSOD dataset and binary-class CMSO dataset (China region).

$$c' = \frac{p_1}{\pi(p_2 + n_2)}. \tag{9}$$

In Eq. (9), π is the snow cover prevalence defined as $\pi = P(sc = 1) = p_2/(p_2 + n_2)$. Note that F_{cpb} is an unbiased estimation of the traditional *F-measure*, and it does not require observed absence data. However, prior information on snow cover prevalence π needs to be acquired beforehand. A straightforward way to get rid of prevalence information to remove the constant c' from Eq. (8), and estimate an approximation of *F-measure* that only requires presence and background data, *i.e.*,

$$F_{pb} = \frac{2 \times TP'}{TP' + FN' + FP'}. \tag{10}$$

In the rest of the paper, we use F to denote the traditional *F-measure* from the presence-absence data, and use F_{cpb} to denote the *F-measure* estimated from presence-background data using Eq. (8), and use F_{pb} to denote the approximation of *F-measure* based on presence-background data using Eq. (8). Note that both F and F_{cpb} are estimating the same accuracy, and F_{cpb} can be regarded as a prevalence-calibrated F_{pb} based on presence-background data.

According to the definition of F_{pb} and its relation to F_{cpb}, the range of F_{pb} is determined by the constant c' defined in Eq. (9), *i.e.*,

$$0 \le F_{pb} \le \frac{2 \times c'}{1 + c'}. \tag{11}$$

Even though the upper bound of F_{pb} depends on the prevalence of snow cover in the study region and the prevalence is usually difficult to acquire, it is useful in practice in terms of ranking models by accuracy and threshold selection. Experiments have demonstrated that F_{pb} is an effective proxy of F (or F_{cpb}) and shows a promising ability to assess the accuracy of binary classification without observed absence data (Li

Table 3
Summary of the training performance of the BP-neural network using different sample populations.

Sampling method	Population of observed presence	Population of background data	Training MSE and Var (75% samples)	Test MSE and Var (25% samples)
#1 one day (Jan 6th, 2006)	500	1500	0.267 (0.039)	0.291 (0.042)
#2 one week (Jan 1st–7th, 2006)	1000	3000	0.201 (0.026)	0.226 (0.032)
#3 half a month (Jan 1st–15th, 2006)	2500	7500	0.172 (0.015)	0.194 (0.019)
#4 one month (Jan 1st–31st, 2006)	5000	15,000	0.153 (0.006)	0.161 (0.009)

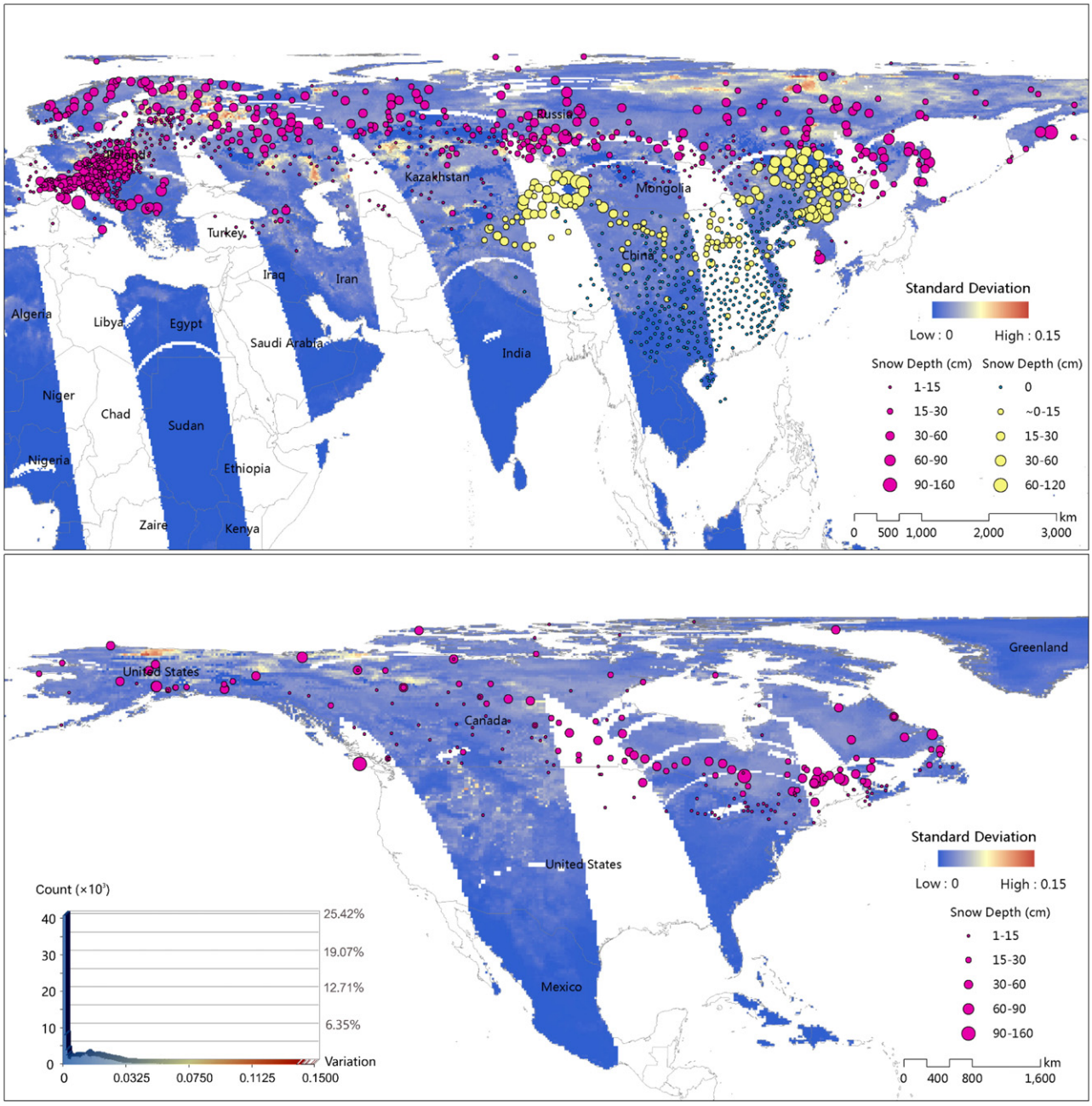

Fig. 6. Standard deviation of 10-time probability predictions on Jan. 6th, 2006, overlapped with ground *in situ* observations. on the embedded plot on the lower left corner presents the histogram of STD of 10-time probability predictions corresponding to the spatial distribution. All plots share the same color ramp.

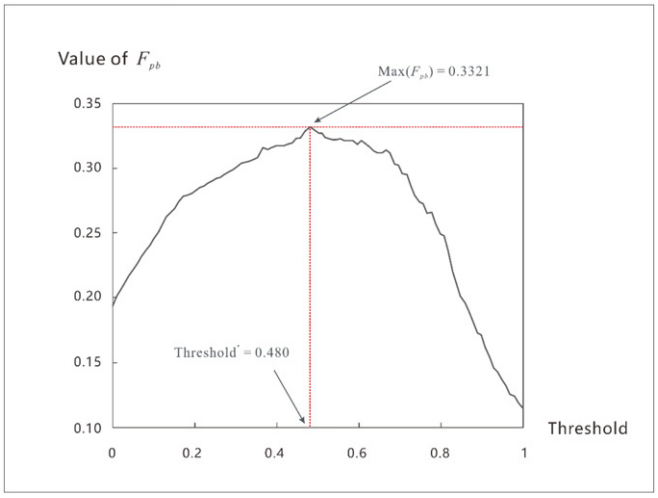

Fig. 7. The variation of F_{pb} over different threshold selections for segmenting the estimated probability of snow cover occurrence on Jan. 6th, 2006. When we select 0.480 as the segmentation threshold, F_{pb} reaches its maximum at 0.3321.

& Guo, 2013, 2014). As to the continuous probability estimated from the PBL model, we can use F_{pb} to compare the binary classification accuracy resulting from different thresholds, and select the best one that can maximize F_{pb} on an independent validation dataset.

5. Model implementation

5.1. Preprocess of input data

In this study, we use SSM/I BTs and their linear combinations as attributes and use the GSOD and CMOS datasets as snow cover labels to train the one-class snow cover estimation model. In order to implement the proposed model, preprocesses are needed to re-label the snow depth records in GSOD and CMOS datasets into binary classes: 'observed snow cover presence label' and 'background label'. Considering that microwave signals response to thinner snow parks at 37GHz are negligible (Kelly et al., 2003), only stations recording >30 mm snow depth are marked as 'observed snow cover presence label'. The observed presence data in the training set are randomly sampled from these stations with observed snow cover label. Note that the background data are randomly sampled from the entire study region, and equivalently can be sample from all stations in the GSOD dataset. All the sampled background data are labeled as "background label" no matter what the original snow depth record is. Similar to previous studies (Derksen, Walker, LeDrew, & Goodison, 2003; Kelly et al., 2003), an assumption is made that snow cover estimated in each SSM/I pixel (25 × 25 km) is equivalent in scale and corresponding to the point observation on the ground. Thus the comparison is on a pixel-wise basis during the sampling process. Previous studies have shown that the BTs data acquired during the afternoon overpass times (descending orbits of the SSM/I sensor) could result in the underestimation of SWE (Derksen, Ledrew, Walker, & Goodison, 2000). Therefore, only BTs acquired from the morning overpass times (ascending orbits of the SSM/I sensor) are used in this study.

5.2. Case-control sampling

In the PBL snow cover estimation model, the training set consists of 'observed snow cover presence' and 'background data'. As mentioned above, these two portions are sampled separately from different populations (case-control sampling). The observed snow cover presences are randomly sampled from stations which observe the snow cover, whereas the background data in the training set are sampled from all stations no matter they record the snow cover or not. The sampling method is applied to the selection of the validation set, too.

Although the GSOD dataset is contributed by >29,000 stations globally (see Fig. 3), only around 600–1000 stations observe the snow cover occurrence per day in winter season, and even less in autumn or spring. Most of these observed presences are dispersedly located in the middle latitude region of the Northern Hemisphere. For example, as shown in Fig. 4, only 926 stations recorded the snow cover presence in Jan. 6th 2006. In the model training process, we found that model training using samples from a single date was usually unstable. This phenomenon exists constantly no matter how we randomly separate the training set and validation set. One might account for this problem is that these observed presences from a single date are not adequate to fully cover the connections between BTs and the probabilities of snow cover occurrence. To address these issues, we implemented different model training configurations by using various sizes of the training set and the validation set sampled from one day, one week, half a months and one month (see more details in Section 6). Besides, the ratio of observed presence samples to background data samples is another factor affecting the model stability. In this study, we set the ratio of observed presence samples to background data samples as 1:3 considering that the snow cover prevalence in the globe is approximately 30% on average.

5.3. Configuration of the BP-neural network

As aforementioned, many binary classifiers are compatible to the PBL model and train the model to conditional probability of snow cover occurrence. In this study we used a backpropagation (BP) neural network to estimate $p_{obs} = P(obs_{sc} = 1|BTs, \eta = 1)$ from the observed presence and background samples. The log-sigmoid function is selected as the transfer function for the model so that the values of estimated probabilities fall within [0, 1]. Mean square errors (MSEs) are used as the objective function in the training process.

In the model training phrase, we randomly selected 25% of the training samples as the test set. The BP-network was run 10 times with different initialization using the rest 75% as the training samples. The average of every sample set over 10 predictions is ranked in descending order. Samples that rank at top percentile, for example 50th percentile, are regarded as members of prototypical presence sample set O, and will be used to estimate the constant c using Eq. (6). After all these steps, the probability of snow cover occurrence p_{sc} can be estimated using Eq. (7).

6. Results and discussions

6.1. Probability estimation of snow cover occurrence

The PBL snow cover estimation model described in section 4 was implemented and applied to SSM/I BT data and GSOD (and CMSO) observations from 1987 to 2010. Fig. 5 presents one selected example illustrating the estimated probability of snow cover occurrence on Jan. 6th 2006. The estimated probability is overlapped with ground *in situ* observations from the GOSD dataset (only presence data) in the globe and the CMSO dataset (both presence and absence data) in China. Note that there are some regions with relatively high estimated probability but no snow cover being recorded in the GSOD dataset. These regions probably correspond to those background data which are actually have snow cover but are not being observed: $obs_{sc} = 0 \cap sc = 1$ (the purple part in Fig. 2).

During the training process, difference sizes of training sample are found to affect the performance of the BP neural network model in estimating the probability of observed snow cover occurrence. We take the date of Jan. 6th 2006 as an example by training the model using various populations of training set: #1 data only sampled from Jan. 6th 2006, #2 data sampled from a week period (Jan. 1st–7th 2006), #3 data sampled from half a month (Jan. 1st–15th 2006), #4 data sampled from the whole month (Jan. 1st–31st 2006). Each model is randomly initialized

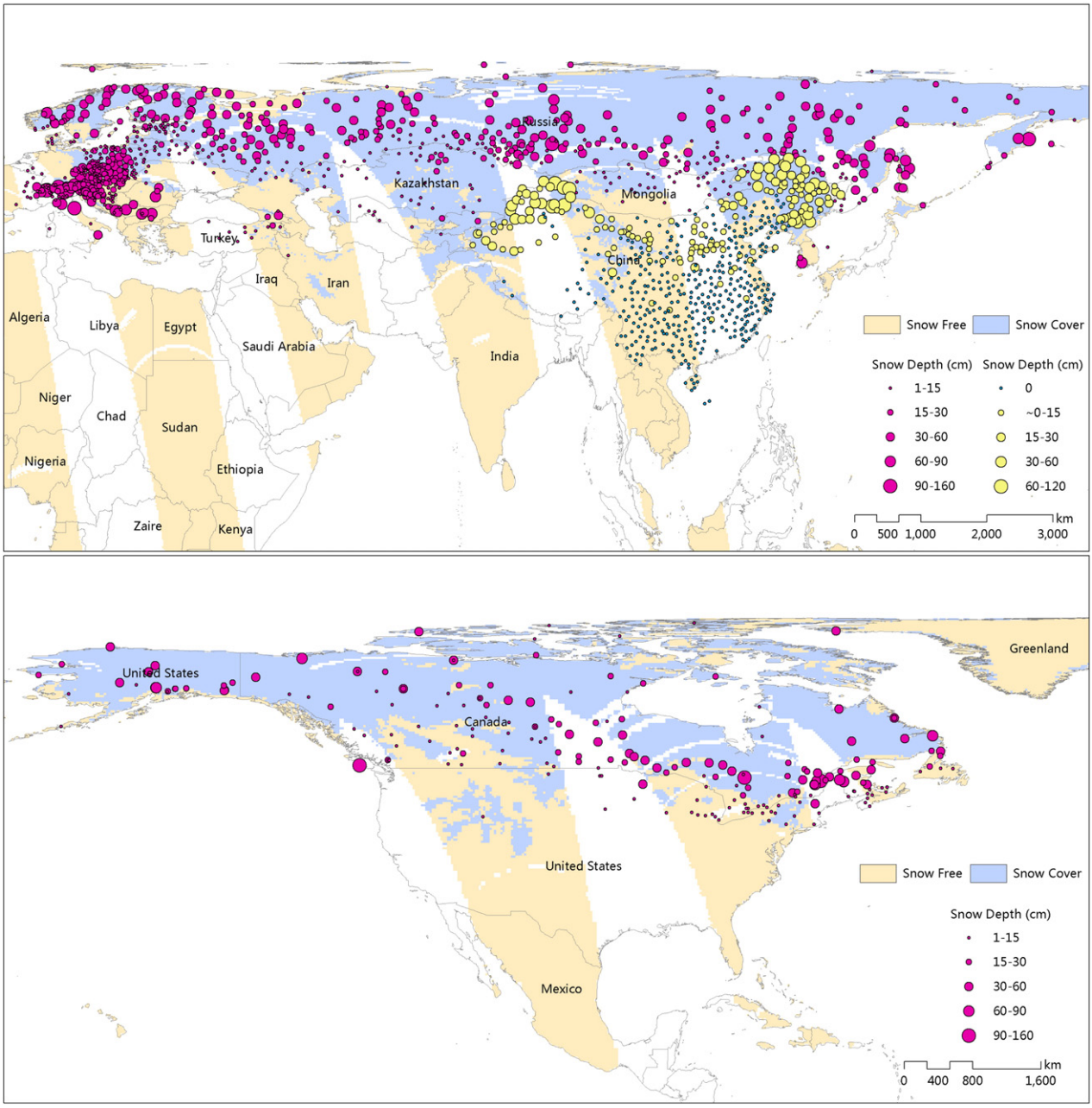

Fig. 8. Probability segmentation using the selected threshold (0.480) that maximize the F_{pb} on Jan. 6th, 2006, overlapped with ground *in situ* observations.

and trained 10 times. The average of 10 mean square errors (MSE) and the variance of these 10 MSEs (Var) are estimated to quantify the model performance. Table 3 summarizes the sampling information and their performance based on the MSE and Var, which are estimated using the training dataset and the validation dataset. From the first row of the table, it shows that if we train the model using 500 observed presences and 1500 background data sampled only from one day, the average and the variance of MSEs are relatively higher in both training (MSE = 0.267, Var = 0.039) and test (MSE = 0.291, Var = 0.042) phases. One possible reason is that 500 observed presences are not adequate to express the relations between SSM/I BTs and the snow cover occurrence probability. By increasing the population of observed presences and background data, this problem could probably be resolved. Unfortunately, observations of snow cover occurrence in a single date is usually <1000 in the winter season and even less in non-winter dates. So we carry out the training phase using observed presences and background data sampled from different length of periods: one week, half a month and a whole month. By training the model with data sampled from a period, uncertainty caused by extreme weather or systematic deviation can be reduced accessorily. As we increase the sample population in the training dataset, both MSE and Var decrease in training and validating phases.

Considering the balance between model performance and training efficiency, a strategy is applied in which we train a monthly model using the training dataset sampled from the whole month, and then use this model to predict the probability of snow cover occurrence on each date of the corresponding month. For example, in January 2006, we trained a model using the dataset sampled from the whole month of January and then predicted the probability of snow cover occurrence using the trained model. Such strategy is applied to every month as long as the SSM/I and ground *in situ* observations are available.

The stability of the predicted probability in terms of spatial distribution is another concern in testing the applicability of the model for long-term snow cover estimation. We trained 10 different models using the

Table 4
Model stability over 10-time snow cover predictions and segmentations on Jan. 6th, 2006.

Segmentation	Snow free (Pixel)	Snow cover (Pixel)	Bias to overlapped region (Pixel, %)	Bias to quantitative average (Pixel, %)	Bias to spatial average (Pixel, %)
#1	108,460	48,879	4,958 (11.29%)	507 (1.05%)	588 (1.22%)
#2	108,161	49,178	5,257 (11.97%)	806 (1.67%)	887 (1.84%)
#3	108,835	48,504	4,583 (10.43%)	132 (0.27%)	213 (0.44%)
#4	109,207	48,132	4,211(9.59%)	−240 (−0.50%)	−159 (−0.33%)
#5	107,441	49,898	5,977 (13.61%)	1,526 (3.15%)	1,607 (3.33%)
#6	110,874	46,465	2,544 (5.79%)	−1,907 (−3.94%)	−1,826 (−3.78%)
#7	107,307	50,032	6,111 (13.91%)	1,660 (3.43%)	1,741 (3.61%)
#8	108,713	48,626	4,705 (10.71%)	254 (0.53%)	335 (0.69%)
#9	109,849	47,490	3,569 (8.13%)	−882 (−1.82%)	−801 (−1.66%)
#10	110,818	46,521	2,600 (5.92%)	−1,851 (−3.83%)	−1,770 (−3.67%)
Overlapped region	–	43,921	–	–	–
Quantitative average	–	48,372	–	–	–
Spatial average	–	48,291	–	–	–

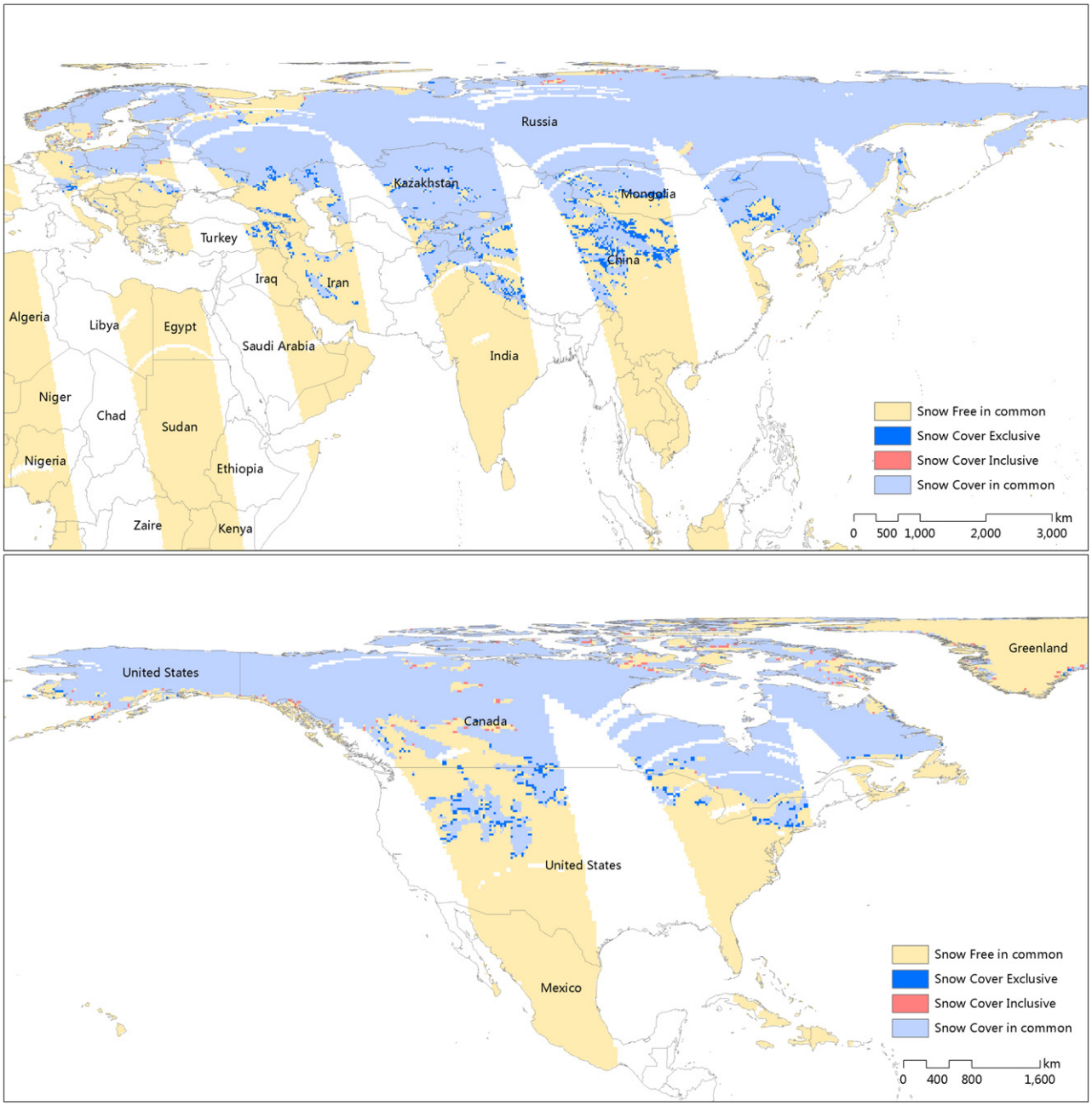

Fig. 9. Comparison of an individual prediction of snow cover with the spatial average of 10-time prediction.

Table 5
Comparison of the predicted snow cover with the observed snow cover presence from the GSOD dataset on Jan. 6th, 2006.

	GSOD dataset (global)	
	Observed snow cover (300)	Observed snow depth >30 mm (200)
Predicted snow cover	263	186
(*Percentage*)	*87.67%*	*93.00%*
Predicted snow-free	37	14
(*Percentage*)	*12.33%*	*7.00%*

Omission error = 0.1233 (0.070 regarding to snow depth >30 mm).

Table 6
Comparison of predicted snow cover with observations from the CMSO dataset on Jan. 6th, 2006.

	CMSO dataset (China region)			
	Snow cover (150)	Snow free (150)	Snow depth >30 mm (100)	Snow free (100)
Predicted snow cover	122	24	92	11
(*Percentage*)	*81.33%*	*16.00%*	*92.00%*	*11.00%*
Predicted snow free	28	126	8	89
(*Percentage*)	*18.67%*	*84.00%*	*8.00%*	*89.00%*

Overall accuracy = 0.8267 (0.9050 when the snow depth >30 mm); Cohen's Kappa coefficient = 0.6533 (0.8100 when the snow depth >30 mm).

training sets randomly sampled from January 2006 and predicted 10 probability results of Jan. 6th 2006. After that, the standard deviation (STD) at each SSM/I grid was estimated according to these 10 predicted probabilities. The spatial distribution of STD is illustrated in Fig. 6, overlapped with ground *in situ* observations from the GSOD dataset and the CMSO dataset. Additionally, the histogram of STD is visualized in the lower left corner of Fig. 6, sharing the same color ramp. Colder colors indicate lower values of STDs in the specific SSM/I grid and hotter colors refer to higher ones. The estimated STD on Jan. 6th 2006 across the globe ranges from 0 to 0.15. Higher STDs are mainly located in regions with high probability of snow cover occurrence but ground *in situ* observations are insufficient (*e.g.*, northern Siberia region and northern Alaska) or observed snow depths are relatively thinner (*e.g.*, eastern Russia and Finland). By examining the distribution pattern of the STD histogram in Fig. 6, we can find that most STDs are smaller than 0.04 (the blue color), of which a majority is very close to 0, meaning that the variation caused by of different training sets and model initializations are relatively small. Moreover, the small number of higher STD (ranging from 0.1 to 0.15) on areas of high predicted probabilities are not supposed to greatly alter the final binary segmentation because the predicted probabilities in these regions are far beyond the segmentation threshold.

6.2. Snow cover segmentation

Following the algorithm described in Section 4.2, the predicted probability of snow cover occurrence needs to be segmented in to binary classes: snow cover and snow-free. The objective of segmentation is to maximize the F_{pb} defined in Eq. (10) based on presence-background data. Ground *in situ* observations, which are independent from the training set, are used to enumerate the values of F_{pb} by choosing the segmentation thresholds ranging from 0 to 1 stepped by an increment of 0.01. Then the threshold that yields the maximum of F_{pb} is used for the probability segmentation. Usually, the threshold determined by observations on the corresponding day wound be ideal for achieving the best accuracy. However, we found that daily observations on the north part of Northern America and Eurasia are relatively rare, leading to unstable segmentation results in these regions. Thus ground observations before and after the specific date are used to select the segmentation threshold. We tried different time periods of 7 days, 15 days, and a month, and found that the thresholds calibrated with 7-day observations can achieve stable performance over tundra areas in a relatively time-saving manner. As to the estimated probability on Jan. 6th, 2006, ground *in situ* observations during Jan. 4th–9th, 2006, which are independent from the training set, are used to select the segmentation threshold for Jan. 6th, 2006. Fig. 7 shows the enumeration of F_{pb} when choosing different thresholds to segment the predicted probability on Jan. 6th 2006. When we selected the value of 0.480 as the segmentation threshold, F_{pb} reaches its maximum at 0.3321. Thus the value of 0.480 is used as the optimum threshold for the segmentation on this date. The result of probability segmentation on Jan. 6th, 2006 is shown in Fig. 8, overlapped with ground observations from the GOSD dataset and the CMSO dataset.

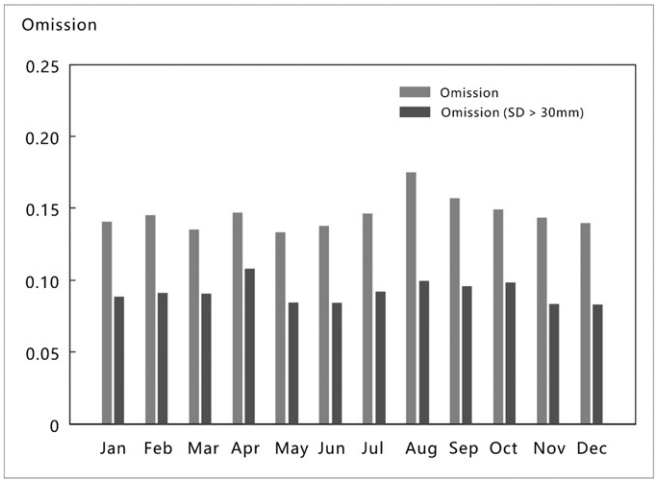

Fig. 10. Monthly omission errors of snow cover estimation during 2006, compared with the GSOD dataset globally.

In order to ensure that the proposed model is applicable to long-term snow cover predictions, the stability of the segmentation results needs to be tested. Similar to the stability test in the probability prediction phase, we trained ten models separately to predicted ten patterns of probability using different training datasets sampled from the same month (January 2006). Then the segmentation phase was carried out to maximize each predicted probability pattern using different test sample sets that are independent from the training sample sets. After that, four statistical metrics including snow cover extent, snow cover overlapped region, quantitative average and spatial average of ten segmentation results were analyzed. The snow cover overlapped region refers to those pixels where all ten segmentations are classified as snow cover. Quantitative average is the algebraic average of the number of pixels to be classified as snow cover among ten segmentations. Spatial average refers to pixels where more than half segmentations are classified as snow cover. Details of ten segmentation results and their biases to the overlapped region, quantitative average and spatial average are summarized in Table 4.

The snow cover extent of ten segmentation results ranges from 46,465 pixels (25 × 25 km grid cell) to 50,032 pixels. The quantitative average (Qua_ave) of ten segmentations is 48,372 pixels, which is calculated directly without consideration for the spatial information. The overlapped region (Ove_region) of ten segmentations contains 43,921 pixels. These regions are expected to have very high confidence to be snow cover since all ten models classify these pixels as snow cover congruously. The spatial average (Spa_ave) of ten segmentations contains 48,291 pixels. More than half of ten models classify these pixels as snow cover and thus these regions are expected to be snow cover averagely. The biases of ten segmentations to Ove_region, Qua_ave and Spa_ave are illustrated in last three columns of Table 4. The bias to Ove_region ranges from 5.79% to 13.91%, which means that we can, in most cases, predict >85% of the snow cover presence with a very high degree of confidence. The bias to Qua_ave and Spa_ave are roughly

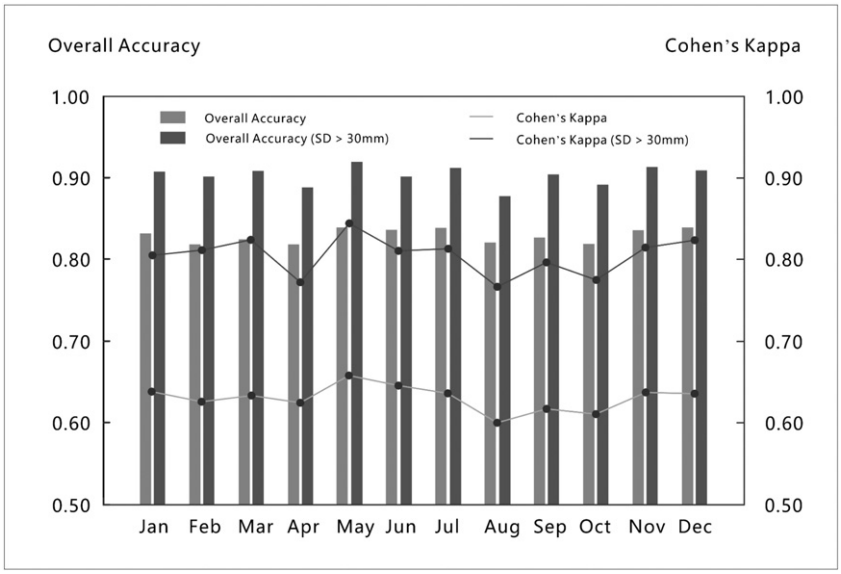

Fig. 11. Monthly overall accuracy and Cohen's kappa coefficient of snow cover estimation in 2006, compared with the CSOD dataset in the China region.

range from 0 to ±4%, which shows the proposed model is stable when applied to snow cover classification.

Fig. 9 illustrates the spatial overlap pattern of #1 segmentation result and the spatial pattern of Spa_ave. Areas covered by the yellow color and light the blue color are predicted to be snow-free and snow cover regions both in #1 segmentation result and the Spa_ave pattern, respectively. Area covered by the dark blue color and the red color are classification disagreements. The dark blue color area is the predicted snow cover included in the #1 segmentation result but not in the Spa_ave pattern, whereas the red color area is the contrary situation, predicted snow cover included in Spa_ave pattern but not in the #1 segmentation result. According to Fig. 9, the extent of areas covered by the dark blue color and the red color is relatively small comparing to the extent of predicted snow cover in common. Most of these inconsistent pixels are mainly scattered around the fringe of large snow cover regions, which, from the spatial perspective, confirms the stability of the proposed model in global snow cover classification.

6.3. Model validation and relative comparisons

6.3.1. Validation using ground in situ observations

The estimated snow cover results are compared with ground *in situ* observations which are sampled from the GSOD dataset but independent from the training set used for the model training phase and the test dataset for binary segmentation phase. Since the GSOD dataset only contains observed presence of snow cover, we simply compare the observed presence with the predicted snow cover. 300 observed presences are randomly sampled from the GSOD dataset on Jan. 6th, 2006, and the observed presences are compared to pixels in which ground stations are located. Table 5 summarizes the comparison between the sampled observed presences and the predicted snow cover results. 247 among 300 validating samples are correctly classified as snow cover, accounting for 82.33% of the validating set. The omission error is 0.177. As we mentioned in the previous section, the pixel-wise comparison between SSM/I grids and station points might introduce uncertainties because an assumption is made that the point observation is equivalent to the whole SSM/I grid. Thus another comparison with station observations is carried that we only select those observed snow depths deeper than 30 mm. 200 observed snow cover records with snow depth >30 mm were randomly sampled from the GSOD dataset from the same date and compared with the model classifications. The omission error significantly decreases to 0.105 (highlight in Table 5), indicating that, as to those areas cover by snowpack, our snow cover estimation results have a promising agreement with ground *in situ* observations.

The monthly omission errors in 2006 are shown in Fig. 10 to examine the agreement between the model results and the ground *in situ* observations during the whole year. Bars in darker color refer to the comparison that only considers observations with snow depth >30 mm. We can see that the omission errors of 12 months are around 0.14 and decrease to around 0.10 regarding to those observations that are cover by snowpack thinner than 30 mm. There is no large variation of omission error showing in the figure, which implies that the proposed method is quite stable when applying to different seasons.

For the China region, the estimation results are compared with the CMSO dataset using both presence and absence observations. The complete binary confusion matrix is created and the overall accuracy and Cohen's kappa coefficient are estimated to quantify the agreement between the ground *in situ* observations and the model results. 300 observation records (150 presences and 150 absences) sampling on Jan. 6th, 2006 are used in the validation process. Similar to the comparison with GSOD dataset, we accessorily carry out another comparison by using observation records with snow depth >30 mm (100 observation records). Table 6 summarizes the details of comparisons. The commission and omission errors are 0.160 and 0.193, respectively in the former comparison (first two columns in Table 6). As to samples with snow depth >30 mm (last two columns in Table 6), the omission error is much smaller (0.090), which indicates the proposed model performs better regarding to areas that are covered by thicker snowpack. The overall accuracy is 0.823 and increases to 0.880 when the snow depth is deeper than 30 mm. The Cohen's kappa coefficients are 0.647 and 0.760,

Table 7
Evaluation of the model performance in snow-melting areas during Jan. 2006.

	GSOD dataset	
	Observed snow cover (200)	Observed snow depth >30 mm (100)
Predicted snow cover	172	87
(*Percentage*)	*86.00%*	*87.00%*
Predicted snow-free	28	13
(*Percentage*)	*14.00%*	*13.00%*

Omission error = 0.140 (0130 regarding to snow depth >30 mm).

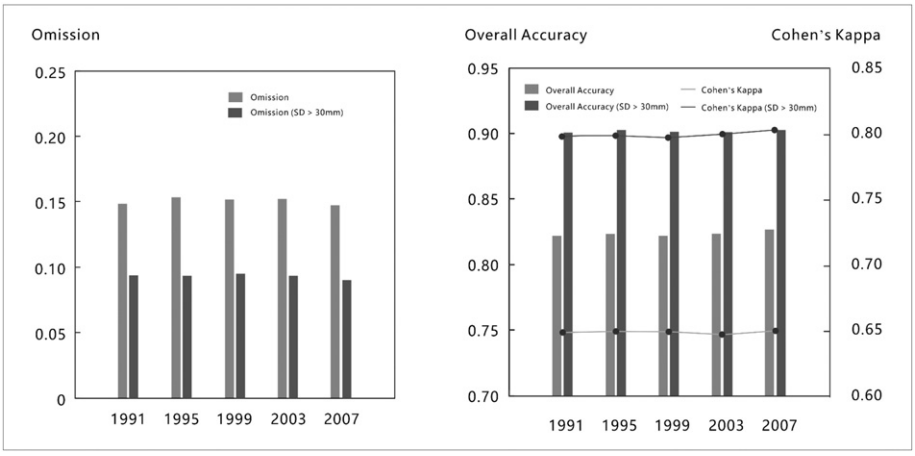

Fig. 12. Yearly omission error (against the GSOD dataset), yearly overall accuracy and Cohen's Kappa coefficient (against the CMSO dataset) of the selected year 1991, 1995, 1999, 2003 and 2007.

respectively, showing substantial agreements between our classification results and ground *in situ* observations in the China region.

The monthly overall accuracy and Cohen's kappa coefficient in 2006 are presented in Fig. 11. Bars and polylines in darker colors refer to the overall accuracy and Cohen's kappa coefficient in a scenario that only considers observations with snow depth >30 mm. The overall accuracies (left vertical axis) of 12 months range from 0.815 to 0.857 and increase to around 0.89 when only consider observations with snow depth >30 mm. The Cohen's kappa coefficients (right vertical axis) of 12 months are around 0.65 and increase to around 0.80 for deeper snow cover with snow depth deeper than 30 mm. Similar to the comparison with the GSOD dataset, the overall accuracy and Cohen's kappa coefficient show no significant variation among 12 months in the China region.

Since the presence of liquid water within the snowpack significantly decreases microwave radiation scattering, traditional methods wound

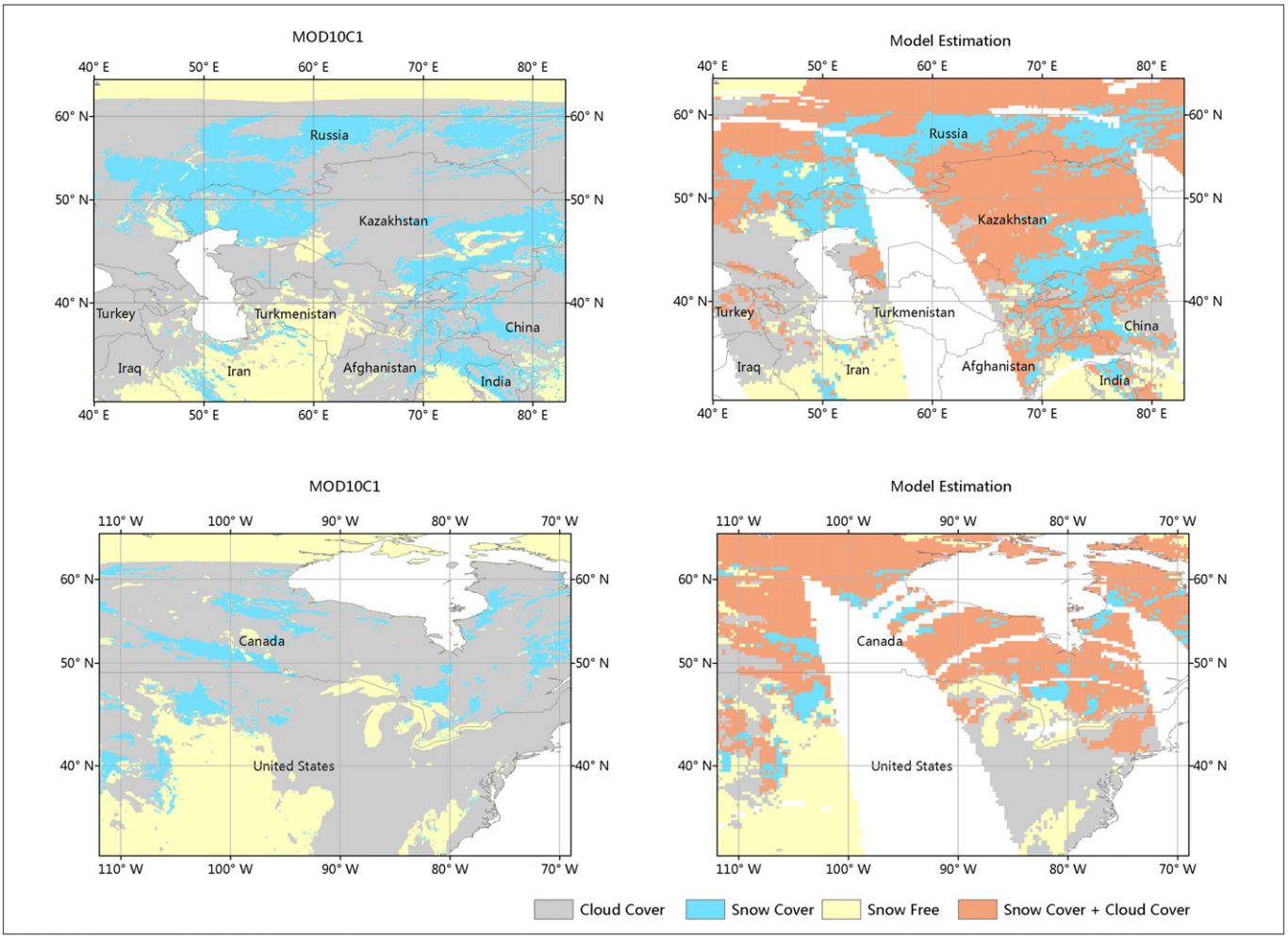

Fig. 13. Comparison of the snow cover area between MODIS daily snow cover product (MOD10C1) and the proposed model prediction under cloud-free condition on Jan. 6th, 2006.

Table 8
Pixel-to-pixel comparison (1000 random samples on each label) between MODIS daily snow cover product (MOD10C1) and the proposed model prediction under cloud-free condition.

	MOD10C1		MOD10C1 resampled	
	Snow cover	Other region	Snow cover	Other region
Predicted snow cover (1000)	868	132	906	93
(*Percentage*)	*86.80%*	*13.2%*	*90.60%*	*9.30%*
Other region (1000)	153	847	114	886
(*Percentage*)	*15.30%*	*84.70%*	*11.40%*	*88.6%*

Overall accuracy = 0.8575 (0.8964 regarding to resampled MOD10C1); Cohen's Kappa coefficient = 0.7150 (0.7929 regarding to resampled MOD10C1).

misclassify the melting snow as snow free. Thus it is necessary to examine the model performance across the melting snow areas. Previous studies have shown that the polarization difference of BT at lower frequencies exhibits a clear discrimination between snow- melting and snow-free areas. In this study we include the polarization difference of BT at 19-GHz and 37-GHz (see Table 1) in the model training and predicting processes. Thus the melting snow should be able to be identified through the trained model. Considering there are no available ground observations of melting snow, we use observations in the GSOD dataset that meets the condition of "snow depth >0 and mean temperature >0" to approximate "melting snow" observations. 200 "melting snow" observations are randomly selected from the GSOD dataset during Jan. 2006, and compare with the model estimations on the corresponding dates. Table 7 present the details of the comparison result. The omission error of the model estimation in melting snow area is 0.140 and slightly better (0.130) in areas with deeper snow cover. The omission errors of melting snow are very close to the performance of overall snow cover evaluation presented in Table 5, which

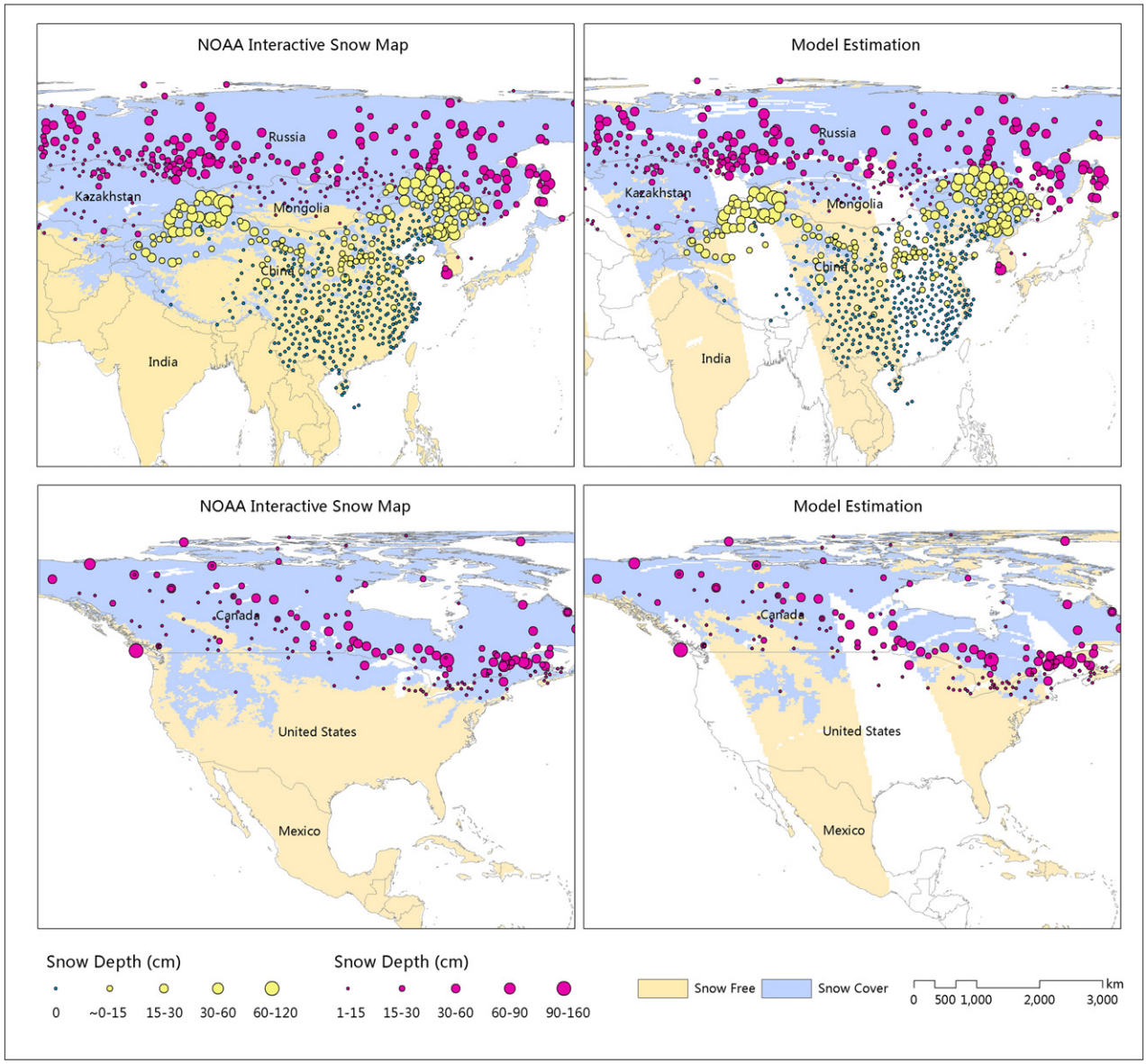

Fig. 14. Comparison between the NOAA daily IMS dataset and the proposed model prediction on Jan. 6th, 2006, overlapped with ground *in situ* observations.

Table 9
Comparison of predicted snow cover and the NOAA daily IMS dataset on Jan. 6th, 2006, using the GSOD and CMSO datasets as references.

	NOAA daily ISM dataset		Model estimation	
	Snow cover	Snow free	Predicted snow cover	Predicted snow free
GSOD dataset (global) Snow cover (300)	269	31	265	35
(*Percentage*)	*89.67%*	*10.33%*	*88.33%*	*11.67%*
CMSO dataset (China) Snow cover (150)	*133*	*17*	129	*21*
(*Percentage*)	*88.67%*	*11.33%*	*86.00%*	*14.00%*
CMSO dataset (China) Snow free (150)	*19*	*131*	*24*	*126*
(*Percentage*)	*12.67%*	*87.33%*	*13.33%*	*86.67%*

Omission error of the NOAA daily ISM dataset is 0.1033, and 0.1167 for our model estimation; Overall accuracy of the NOAA daily ISM dataset is 0.8800, and 0.8500 for our model estimation; Cohen's kappa coefficient of the NOAA daily ISM dataset is 0.7600, and 0.7000 for our model estimation.

means the proposed method can successfully identify snow cover over melting snow areas.

In order to examine the applicability and the performance of the proposed method in a long term period, five years in the study period (1991, 1995, 1999, 2003, 2007) are selected to evaluate the omission error against the GSOD dataset in the globe, and the overall accuracy and Cohen's kappa coefficient against the COSD dataset in the China region. Fig. 12 presents the assessment statistics of the selected years.

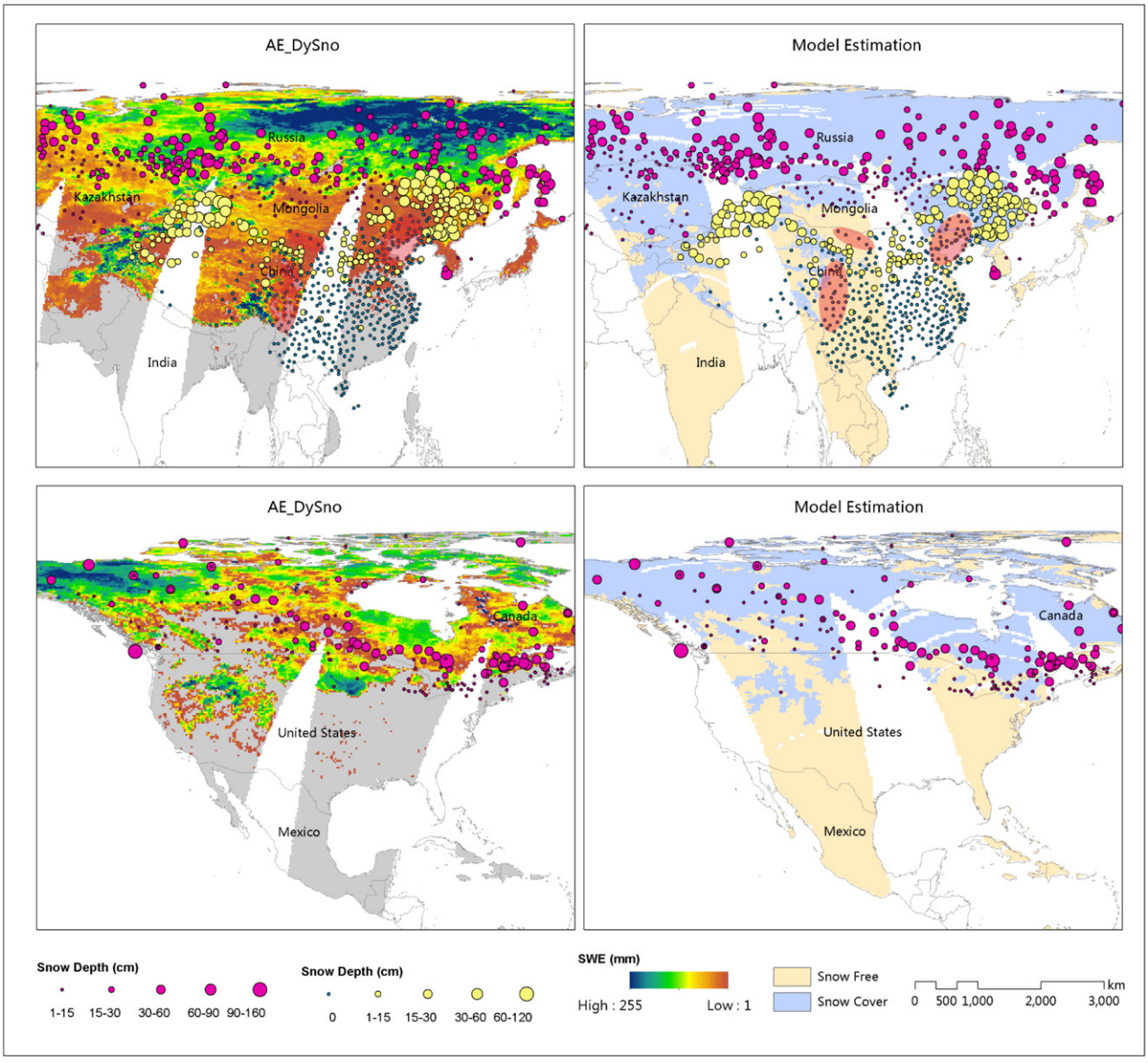

Fig. 15. Comparison between the AMSR-E daily SWE product (AE_DySno) and the proposed model prediction on Jan. 6th, 2006, overlapped with ground *in situ* observations. Areas highlighted with translucent-red ellipses indicate the overestimation of the AE_DySno dataset.

Table 10
Comparison of the predicted snow cover and the AE-DySno SWE dataset on Jan. 6th, 2006, using the CMSO dataset as references.

	CMSO dataset (China region)	
	Snow cover (150)	Snow free (150)
Predicted snow cover	125	26
(*Percentage*)	*83.33%*	*17.33%*
Predicted snow free	25	124
(*Percentage*)	*16.67%*	*82.67%*
AE_DySno SWE > 0	*129*	*41*
(*Percentage*)	*86.00%*	*27.33%*
AE_DySno SWE = 0	21	109
(*Percentage*)	*14.00%*	*72.67%*

Overall accuracy of the model estimation = 0.830, Overall accuracy of AE_DySno = 0.7933; Cohen's Kappa coefficient of the model estimation = 0.660, Cohen's Kappa coefficient of AE_DySno = 0.5867.

Overall, these statistical results are quite stable, and keep consistent with that of 2006. The omission errors evaluated against the GSOD dataset range from 0.17 to 0.18, and decrease to around 0.11 for station observations with snow depth >30 mm. The overall accuracies and Cohen's kappa coefficients evaluated against the COSD dataset in the China region are stable at 0.82 and 0.65 respectively, and increase to 0.88 and 0.76 for station observations with snow depth >30 mm. Since the proposed PBL-based model adaptively calibrates daily snow cover using the corresponding daily ground observations, the proposed method shows to be applicable for a long-term period considering the promising performance in 2006 and the stable statistics of assessment in other six years.

6.3.2. Comparison with MODIS snow cover product (MOD10C1) in the Northern Hemisphere

The estimation results are compared with the extensively-used Moderate Resolution Imaging Spectroradiometer (MODIS) snow cover product (MOD10C1). The MOD10C1 product is a daily global climate modeling grid (0.05°) dataset based on the vis-IR spectrum reflectance retrievals, more specifically, based on the Normalized Difference Snow Index (NDSI) algorithm (Hall, Salomonson, & Riggs, 2006). However, optical sensors cannot observe the earth's surface when clouds or darkness are present. Thus only in regions where are cloud-free and illuminated by sunlight, the MOD10C1 dataset is capable to distinguish whether the earth surface is covered by snowpack or not. So the comparison is only focused on areas where snow cover in the MOD10C1 dataset is dominant (100%). By using the cloud cover and seasonal darkness area in the MOD10C1 dataset, the classification results and the MOD10C1 snow cover region are masked and relabeled into four categories: “snow cover”, “cloud cover”, “snow free” and “snow cover + cloud cover”. The “snow cover + cloud cover” category only exists in our model estimations (right column), indicating areas that are predicted to be snow cover but are covered by cloud. Fig. 13 shows the patterns of the MOD10C1 snow cover (left) and the model classification results (right) in two selected regions (around 60°E-50°N and 90°W-50°N) on Jan. 6th 2006. Despite differences in spatial resolutions, the pattern of snow cover in the model classification result (blue color area) is highly comparable to that of the MOD10C1 dataset. A pixel-to-pixel comparison is performed on these reclassified labels to examine the agreement of the snow cover pattern under cloud-free areas. We merged the “cloud cover”, “snow free” and “snow

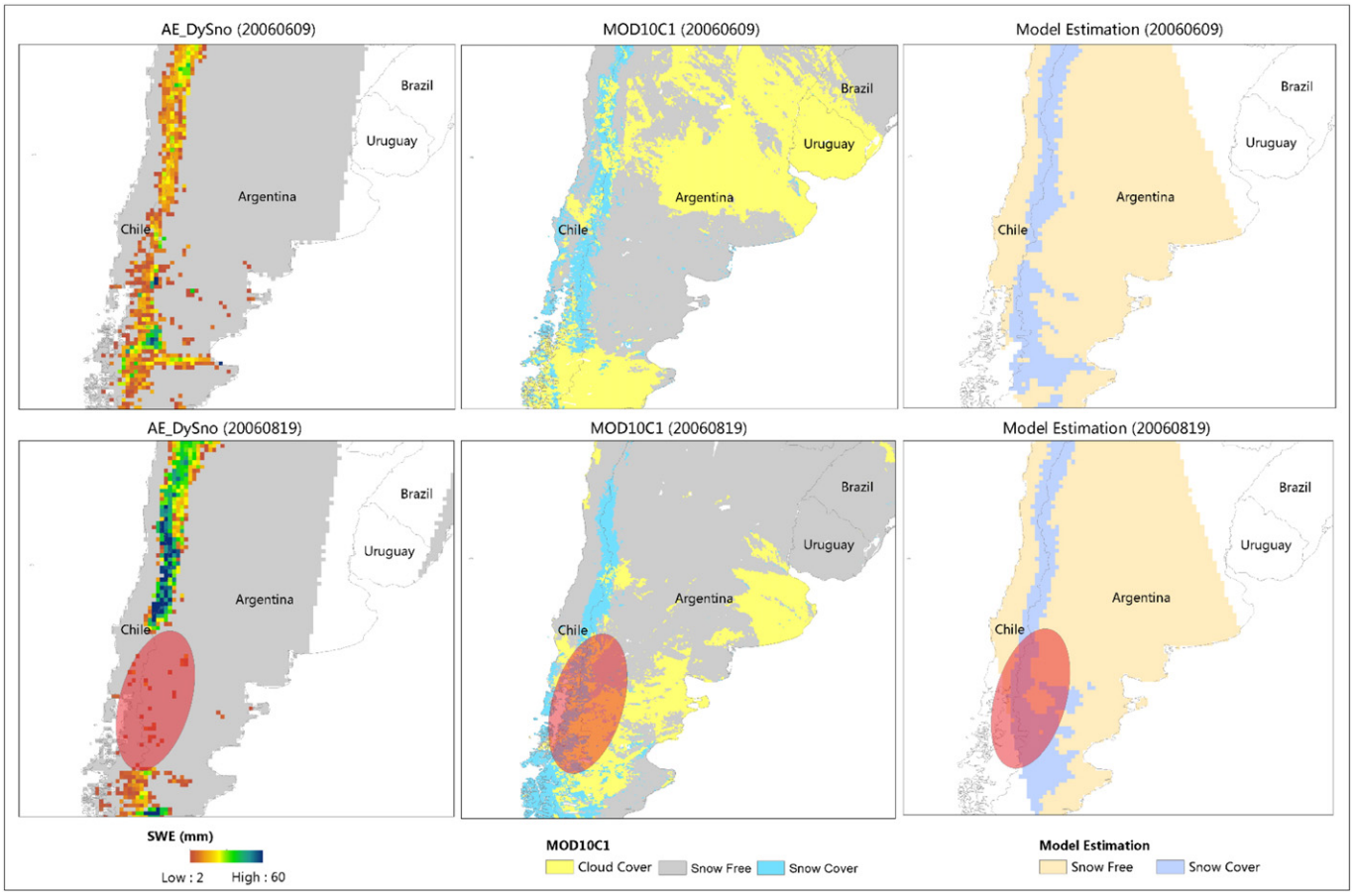

Fig. 16. Comparison of our predicted snow cover pattern with the AE_DySno SWE product and the MOD10C1 dataset in the Chile-Argentina area in winter season in the Southern Hemisphere (Jun. 9th, 2006 and Aug. 19th, 2006).

Table 11
Comparison of the estimated snow cover with the MOD10C1 snow cover dataset and the AE_DySno SWE dataset on Jun. 9th and Aug. 19th, 2006, using MOD10C1 as reference (50 samples each day).

	AMSR-E		Model estimation	
	SWE > 0	SWE = 0	Snow cover	Snow free
MOD10C1 snow cover (Jun 9th)	41	9	42	8
(*Percentage*)	*82.00%*	*18%*	*84%*	*16%*
MOD10C1 snow cover (Aug 19th)	34	16	40	10
(*Percentage*)	*68%*	*32%*	*80%*	*20%*

cover + cloud cover" arears into one label of "other region", and then randomly generated 1000 points on each label to examine the agreement between the two classified results. To eliminate the influences of spatial resolution between two compared datasets, another comparison is carried out in which the MOD10C1 snow cover dataset is resampled into the same resolution (25 × 25 km). Table 8 summarizes the details of two comparisons between these two classified results.

The overall accuracy is 85.75% in the original comparison and reaches 89.64% when the MOD10C1dataset is resampled into coarser resolution. The Cohen's kappa coefficients are 0.7150 and 0.7929, respectively. Both the overall accuracy and Cohen's kappa coefficient indicate that the model classification agrees well with the MOD10C1 dataset in cloud-free areas.

6.3.3. Comparison with NOAA IMS Dataset in the Northern Hemisphere

The estimation result based on the proposed method is compared to the NOAA daily Interactive Multisensor Snow and Ice Mapping System (IMS) dataset created by the National Ice Center (National Ice Center, 2008). This dataset provides snow and ice cover maps for the Northern Hemisphere from February 1997 to present. It is derived from a variety of data products including satellite imagery and *in situ* data, and gridded in three different spatial resolutions: 1 km, 4 km, and 24 km. Since the spatial resolution of our model estimation is 25 km, the NOAA daily IMS dataset of 24 km is used in this comparison. Fig. 14 presents the snow cover pattern of the NOAA daily IMS dataset (left) and our model estimation (right) in the Northern Hemisphere on Jan. 6th 2006, overlapped with ground *in situ* observations from the GSOD and CMSO datasets. Overall the two snow cover patterns are quite similar at a continental scale, especially in Eurasia. Somehow the proposed method seems to estimate relatively generate less snow cover extent along the boundary of Canada and the USA (see the button row of Fig. 14) as compared to the NOAA daily IMS dataset. In order to quantitatively examine the agreement between these two snow cover patterns against ground observations, we selected 1000 observations from the GOSD dataset and 300 (150 snow cover and 150 snow free) from the CMSO dataset to establish the confusion matrix and evaluate the omission error, the overall accuracy and Cohen's kappa coefficient. Table 9 summarizes the details of the quantitative comparisons. The omission errors globally evaluated against the GSOD dataset are 0.1033 for the NOAA daily IMS dataset and 0.1167 for the model estimation, respectively. The overall accuracy and Cohen's kappa coefficient of the NOAA daily IMS dataset in China are slightly better than these of our model estimation, too (overall accuracy: 0.8800 *vs* 0.8500, Cohen's kappa coefficient: 0.7600 *vs* 0.7000). All three assessment statistics indicate promising accuracy of these two snow cover patterns. Even though the NOAA daily IMS dataset is derived from various satellite imageries and ground *in situ* data, the proposed method can still achieve good agreement with the NOAA daily IMS dataset.

6.3.4. Comparison with AMSR-E daily snow product in the Northern Hemisphere

The estimation results based on the proposed method are further compared to another snow cover dataset: the AMSR-E daily snow product (AE_DySno). The AE_DySno dataset is a global estimation of snow cover and SWE using multi-frequency passive microwave BT data acquired from the Advanced Microwave Scanning Radiometer-Earth Observing System (AMSR-E) (Tedesco et al., 2004). Fig. 15 shows the AE_DySno SWE pattern (left) and our model classification (right) on Jan. 6th, 2006, overlapped with ground *in situ* observations. Colder colors indicate higher SWE estimation in the AE_DySno dataset. If consider snow cover extent as the areas where SWE > 0, we find that the snow cover extent indicated by AE_DySno is obviously larger than that of our model classification results. We compared these two estimations in the China region where both observed presence and absence data are available to figure out whether the PBL-based results are underestimated or not. In regions that are observed to be snow-free (covered by small blue dots and highlighted with translucent-red ellipses), the AE_DySno dataset is found to have SWE > 0, despite SWE in these regions are relatively small. But our model classification shows better agreement with the ground *in situ* observations.

In order to quantitatively investigate this phenomenon, 300 observation records (150 presences and 150 absences) on Jan. 6th, 2006 are from the GSOD dataset to quantify the agreement of two datasets to the ground *in situ* observations in the China region. Table 10 summarizes the details of the comparison. 41 of 150 snow-free samples correspond to the pixels where SWE > 0 in AE_DySno dataset. Although the omission error of the AE_DySno (0.140) is slightly lower than that of our model estimation results (0.1667), the commission error of the AE_DySno dataset is much higher (0.2733 comparing to 0.1773). The reason is that the AE_DySno dataset seems to overestimate the SWE on some snow-free regions in China (highlighted with translucent-red ellipses in Fig. 15). As a result, relatively more snow-free ground observations are misclassified as "snow cover", contributing to the higher commission error. From Table 10 we can see that both the overall accuracy and Cohen's kappa coefficient of our model estimation are superior to the AE_DySno. All these quantitative analyses confirm the indication of Fig. 15 that our model estimation agrees better with the ground *in situ* observations in regions with thinner snow cover.

6.3.5. Comparisons in the Southern Hemisphere

Compared to the Northern Hemisphere, the snow cover extent in the Southern Hemisphere is rather small even though in the winter season (from June to September). Surface snows are mainly located along the boundary between Chile and Argentina (Andes mountain range) and on the south part of the Patagonia Plateau. In these regions there are no available ground observations in the GSOD dataset. Thus in the South Hemisphere we verify the proposed method by comparing the estimated snow cover patterns with the MOD10C1 and AE_DySno datasets. The MOD10C1 snow cover under clear-sky conditions are considered to be the reference, and the SWE patterns of AE_DySno are used to relatively validate the estimated snow cover pattern where the cloud cover is present.

It is not easy to find dates when all three sensors simultaneously cover the southern Andes mountain range and few cloud cover is present. Fig. 16 presents two groups of comparative snow cover patterns on Jun. 9th (above row of Fig. 16) and Aug. 19th (bottom row Fig. 16) of 2006 when all three sensors covered the southern Andes mountain range and as few cloud cover as possible. We can observe from Fig. 16 that, in general, the snow cover patterns of the AE_DySno dataset, the MOD10C1 dataset and our model estimation are quite similar. Compared to the optical-based MOD10C1 dataset, both BT-based retrieval methods are fail to identify snow shatters on the seashore of Chile. On both Jun. 9th and Aug. 19th, the surface snows are mainly located along the boundary of Chile and Argentina and in the Patagonia Plateau. On date Aug19th, the AE_DySno daily SWE dataset seems to underestimate the snow cover areas on the Patagonia Plateau (highlighted by a translucent-red ellipse in Fig. 14), while our estimated snow cover pattern is matched well with the MOD10C1 snow cover pattern in cloud-free areas.

To quantitatively illustrate the agreements among the snow cover patterns of the MOD10C1 dataset, the AE_DySno dataset and the model estimation, we randomly select 50 samples each day from the snow cover region in the MOD10C1 dataset as references, and examine whether the selected samples are classified as snow cover (or SWE > 0) in our estimated results and the AE_DySno dataset. In this way, we can approximately derive the commission errors of the estimated snow cover pattern and compare it with that of the AE_DySno dataset. The details of comparison are shown in Table 11. On Jun. 9th, 41 of 50 (82%) samples are labeled as SWE > 0 in the AE_DySno dataset, while our model estimation is slightly better, with 42 (84%) are labeled as snow cover. On Aug. 19th, only 34 (68%) samples are found to be SWE > 0 in the AE_DySno dataset due to underestimation on the Patagonia Plateau. In comparison, the proposed estimation model is more stable, by which 40 of 50 (80%) samples are classified as snow cover.

6.4. Limitations and future studies

Traditional microwave BT-based methods usually do not perform very well in identifying snow cover on ice sheet and glacier regions such as Greenland and Antarctica. In the AMSR-E daily SWE dataset (AE_DySno), almost all of Greenland and Antarctica are labeled as "ice sheet" instead of "snow cover". However, in the NOAA Interactive Snow Cover Map (NOAA IMS), the Greenland is labeled as "snow cover". According to the estimation from the proposed method, snow cover probabilities in the Greenland and Antarctica are rather small. Since we do not have adequate ground observation in these two areas, we excluded them from our model estimation, and labeled them as "not estimated" in the final results. In future work, more efforts will be applied to study the snow cover identification on the ice floors.

Accurate long-term series of daily snow cover datasets are valuable for modeling global climate change and test climate model simulations. Following this study, it would be interesting to apply the proposed model to the Scanning Multichannel Microwave Radiometer (SMMR) BT data ad extend the time series of the products back to 1978, since the frequencies of the SMMR BT data are very similar to that of the SSM/I and the daily ground observations are available during the same time period.

Although historical snow cover extents are estimated using the proposed method, it is difficult to derive the time-series trend of snow cover extents during long-term period based only on these daily snow cover estimations, because the tiles of the SSM/I sensors are only cover parts of the globe every day and the footprint keeps changing continuously. In future studies, we may need to integrate the daily snow cover estimations into 5-day, weekly, or 8-day compositions of snow cover extents after extensive validations of daily results against ground *in situ* observations. These compositions, which can fully cover the whole globe in one scene, will be useful to derive the historical trend of the snow cover extent during the past 30 years for further global climate applications.

7. Conclusion

Current microwave-based methods of global snow cover estimation are found to be spatial and temporal bias, because the heterogeneity of snowpack and land cover are not fully considered in these stand-alone algorithms. Regression coefficients in such empirical algorithms are usually calibrated by insufficient ground observations of snow information. Thus the accuracy is greatly dependent on local conditions and scene characteristics, limiting the model applicability for deriving promising snow cover products in a long-term period.

This study presents an approach to determine global snow cover extent by combining space-borne microwave measurement and daily ground *in situ* snow cover observations. The novelty of the proposed method is that the adopted PBL algorithm can be trained and used to identify snow cover only using observed snow cover presence records, considering that consistent station observations of snow-free records on a global scale are usually unavailable. Because the proposed model utilizes ground observations and microwave measurements on a daily basis, it is temporally and spatially dynamic such that estimation errors are independent of local conditions and scene characteristics.

The model stability in both the training phase and the segmentation phase is tested by examining the variation across 10-time independent model training and segmentation. The standard deviation of 10-time estimated probabilities across the globe ranges from 0 to 0.15, of which a majority is very close to 0. The bias of the ten-time segmentation results to the quantitative-average and spatial-average roughly range from 0 to $\pm 7\%$. The results of these tests confirm the stability of the proposed model in global snow cover estimation, both in spatial and quantitative perspectives. Areas with higher uncertainties are mainly located in the regions that have fewer ground *in situ* observations or are scattered around the fringe of large snow covered regions.

The proposed model is implemented and applied to the estimation of global snow cover from 1987 to 2010, using BT measurements from SSM/I instrument and daily ground snow cover observations from the GSOD and CMSO datasets. The estimation results are validated against ground *in situ* observations and compared with the MODIS daily snow cover product (MOD10C1), the NOAA IMS dataset and AMSR-E daily SWE dataset (AE_DySno). The global omission error of the snow cover estimation on Jan. 6th, 2006 is 0.1233. The overall accuracy and Cohen's kappa coefficient on the same date in the China region are 0.8265 and 0.6533, respectively. If we only consider scenarios that snow depth >30 mm, the global omission reduces to 0.07, and the overall accuracy and kappa increase to 0.905 and 0.810, respectively. The above statistics are also evaluated in monthly average during 2006. The monthly omission error of the snow cover estimation is around 0.14 and reduces to 0.10 when only considering observations with snow depth >30 mm. The monthly overall accuracy and Cohen's kappa coefficient in the China region are around 0.83 and 0.65, and increase to 0.89 and 0.80 when only considering observations with snow depth >30 mm, respectively. All these statistics show no significant variation over12 months in 2006, and the same as that of the other five selected years (1991, 1995, 1999, 2003, and 2007), indicating that the proposed method not only achieves promising accuracies, but also shows stable when applying to different seasons and years. The comparison between the model estimation and the MOD10C1 products shows good agreement under cloud-free conditions. The comparison between the model estimation against the NOAA IMS dataset also shows promising agreement in the Northern Hemisphere. Another comparison of our model results with the AE_DySno dataset demonstrates the benefits of the proposed method regarding to the overestimation problem in regions with thinner snow cover.

Similar to traditional microwave BT-based methods, the proposed method does not perform very well in identifying snow cover in regions with ice sheets and glaciers such as Greenland and Antarctica. These two areas are excluded from our model estimation, and are labeled as "not estimated" in the final results. In the future work, more efforts need to be made to identify snow cover on the ice floors.

Acknowledgments

This study was supported by the National Science Fund for Excellent Young Scholars (Grant No. 41322009), the Key National Natural Science Foundation of China (Grant No. 41531176), and the National Natural Science Foundation of China (Grant No. 41371376).

Appendix A. Additional estimated snow cover patterns in Jan. 2006

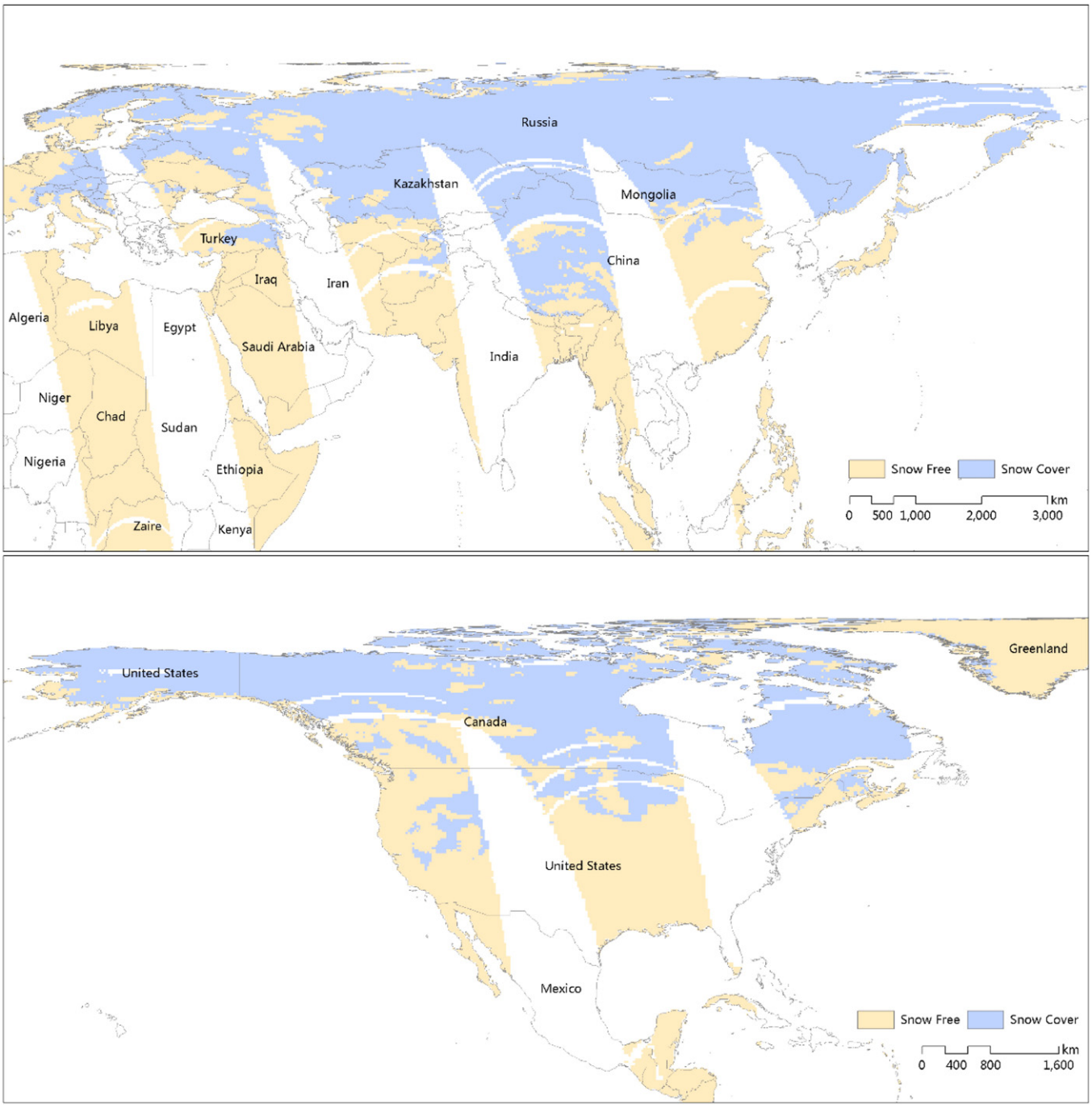

Fig. A1. Estimated snow cover pattern on Jan. 10th, 2006.

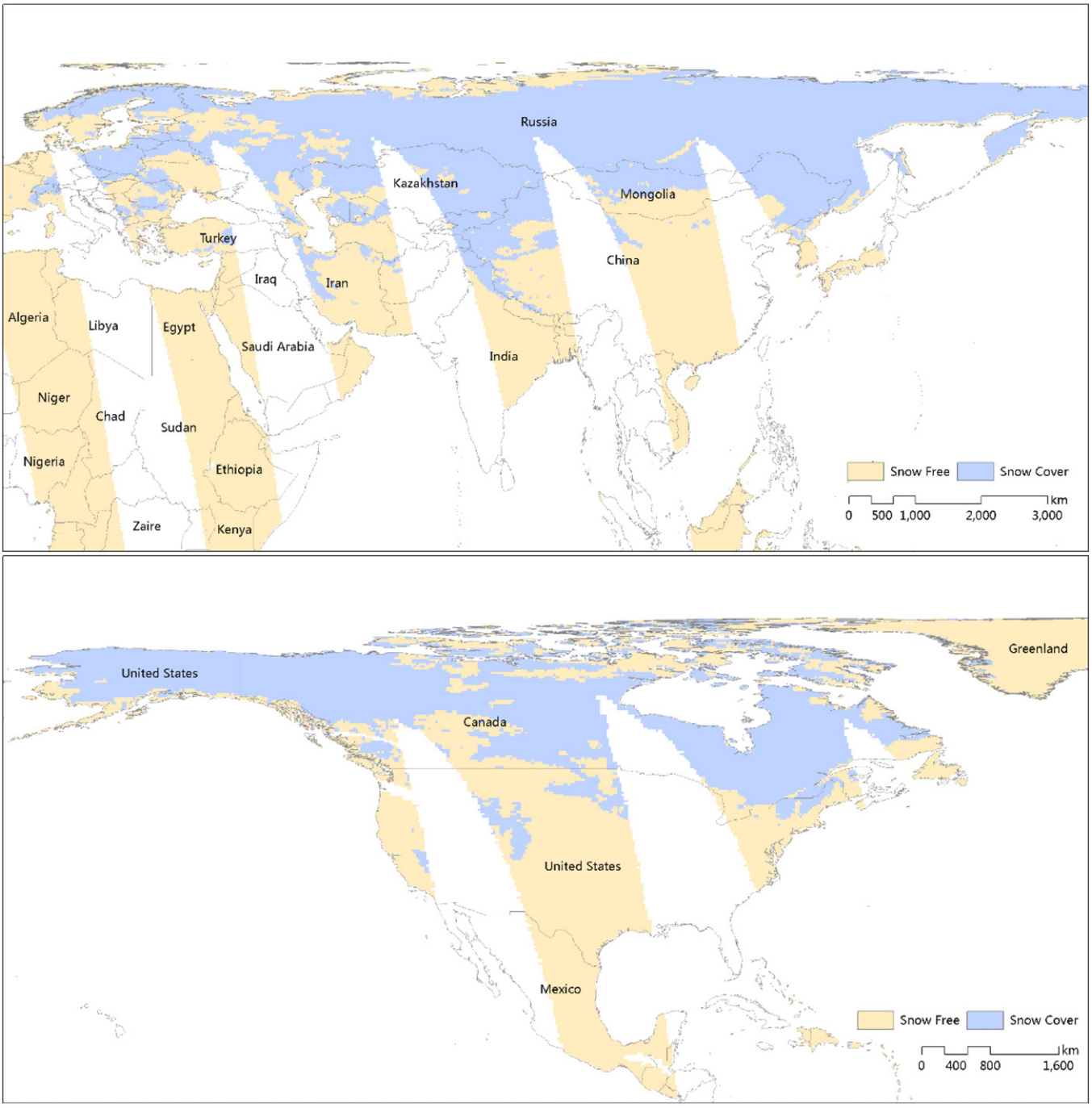

Fig. A2. Estimated snow cover pattern on Jan. 15th, 2006.

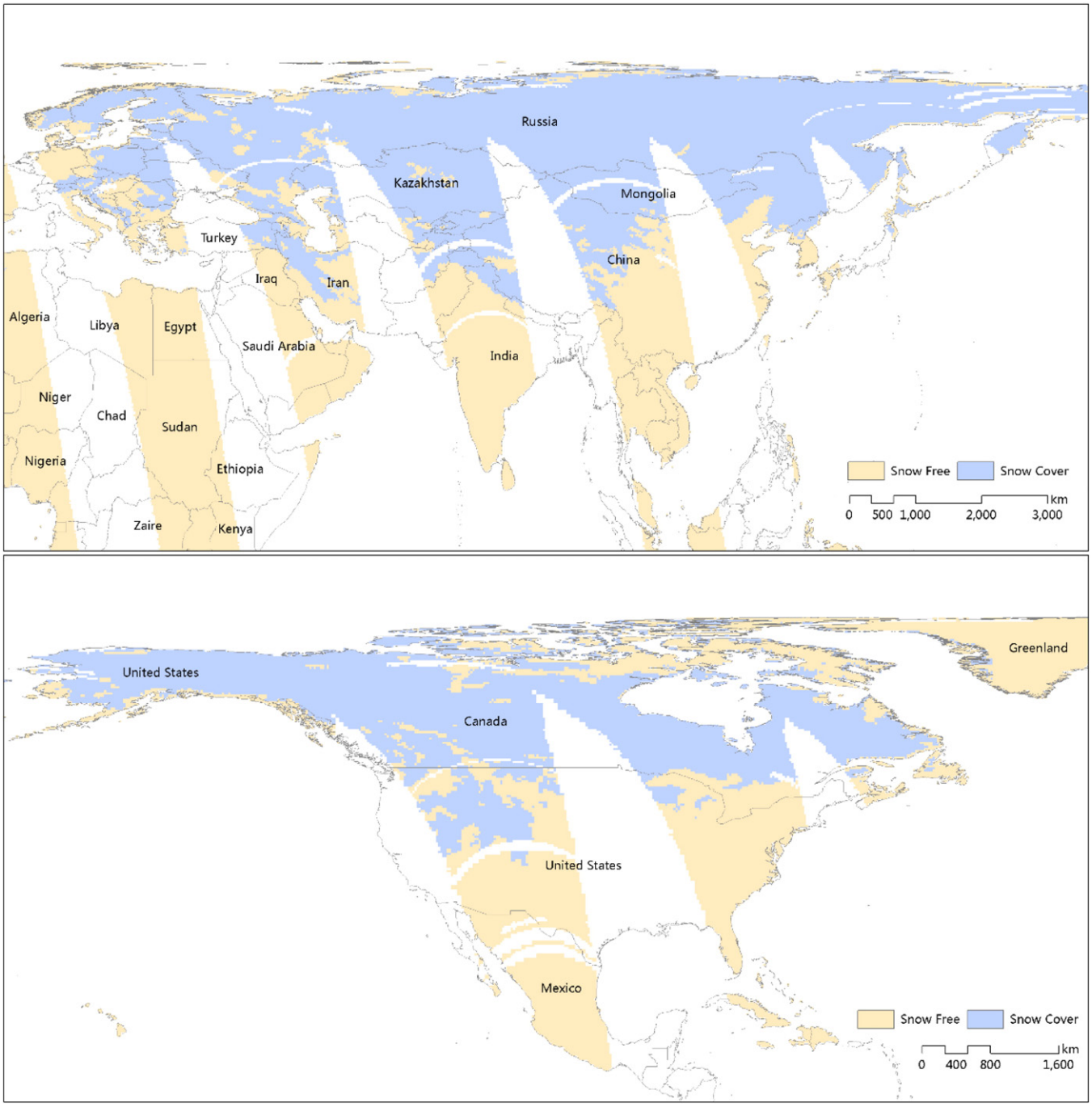

Fig. A3. Estimated snow cover pattern on Jan. 20th, 2006.

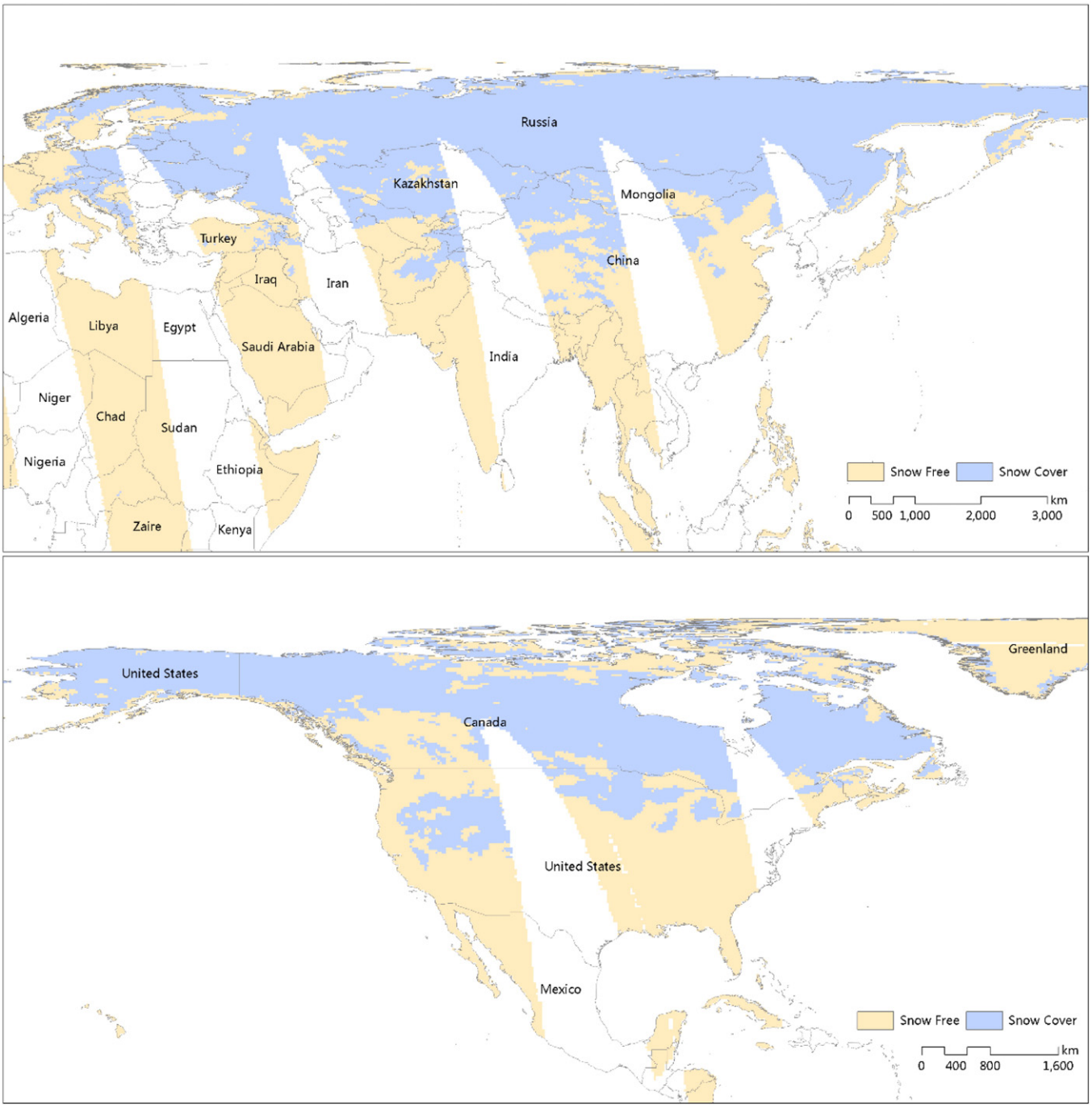

Fig. A4. Estimated snow cover pattern on Jan. 25th, 2006.

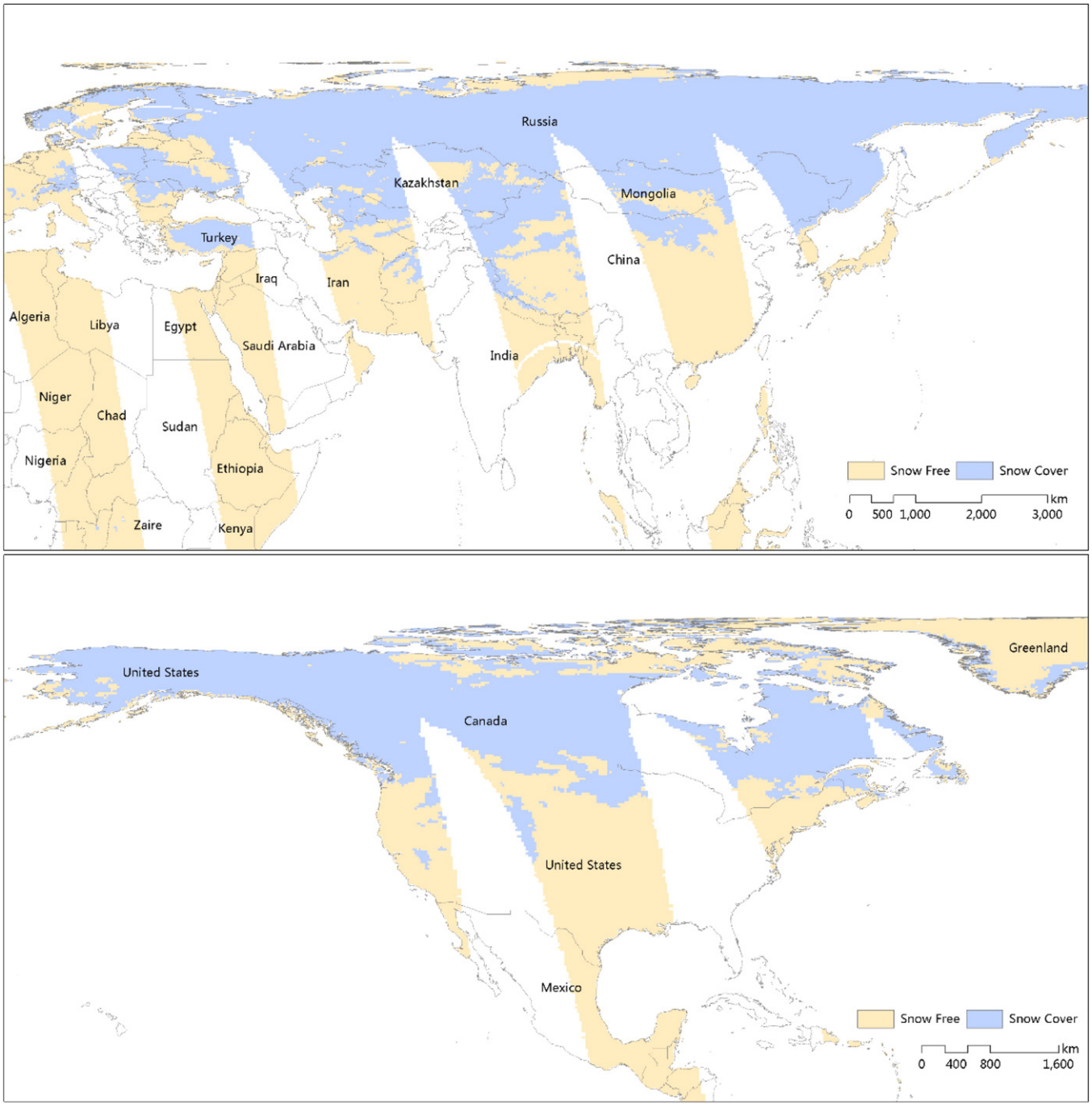

Fig. A5. Estimated snow cover pattern on Jan. 30th, 2006.

Appendix B. Supplementary data

Supplementary data to this article can be found online at http://dx.doi.org/10.1016/j.rse.2016.05.010.

References

Allan, F., & David, A. R. (1999). Northern hemisphere snow extent: regional variability 1972–1994. *Int. J. Climatol., 19*, 1535–1560.

Allen, R. C., Durkee, P. A., & Wash, C. H. (1990). Snow/cloud discrimination with multispectral satellite measurements. *J. Appl. Meteorol., 29*, 994–1004.

Armstrong, R., Knowles, K., Brodzik, M., & Hardman, M. A. (1994). *DMSP SSM/I-SSMIS pathfinder daily EASE-grid brightness temperatures, version 2.* Colorado USA. NASA National Snow and Ice Data Center Distributed Active Archive Center: Boulder. http://dx.doi.org/10.5067/3EX2U1DV3434 (updated 2015).

Armstrong, R. L., & Brodzik, M. J. (1995). An earth-gridded SSM/I data set for cryospheric studies and global change monitoring. *Adv. Space Res., 16*, 155–163.

Chang, A., Foster, J. L., Hall, D. K., Rango, A., & Hartline, B. K. (1982). Snow water equivalent estimation by microwave radiometry. *Cold Reg. Sci. Technol., 5*, 259–267.

Chang, A., Foster, J. L., & Hall, D. K. (1987). Nimbus-7 SMMR derived global snow cover parameters. *Ann. Glaciol., 9*, 39–44.

Cohen, J. (1960). A coefficient of agreement for nominal scales. *Educ. Psychol. Meas., 20*, 37–46.

Cohen, J., & Entekhabi, D. (1999). Eurasian snow cover variability and northern hemisphere climate predictability. *Geophys. Res. Lett., 26*, 345–348.

Congalton, R. G. (1991). A review of assessing the accuracy of classifications of remotely sensed data. *Remote Sens. Environ., 37*, 35–46.

Derksen, C., Ledrew, E., Walker, A., & Goodison, B. (2000). Influence of sensor overpass time on passive microwave-derived snow cover parameters. *Remote Sens. Environ., 71*, 297–308.

Derksen, C., Walker, A., LeDrew, E., & Goodison, B. (2003). Combining SMMR and SSM/I data for time series analysis of central north American snow water equivalent. *J. Hydrometeorol., 4*, 304–316.

Foster, J. L., Chang, A., & Hall, D. K. (1997). Comparison of snow mass estimates from a prototype passive microwave snow algorithm, a revised algorithm and a snow depth climatology. *Remote Sens. Environ.*, *62*, 132–142.

Grody, N. C. (1991). Classification of snow cover and precipitation using the special sensor microwave imager. *J. Geophys. Res. Atmos.*, *96*, 7423–7435.

Grody, N. C., & Basist, A. N. (1996). Global identification of snowcover using SSM/I measurements. *IEEE Trans. Geosci. Remote Sens.*, *34*, 237–249.

Hall, D. K., Riggs, G. A., Salomonson, V. V., Digirolamo, N. E., & Bayr, K. J. (2002). MODIS snow-cover products. *Remote Sens. Environ.*, *83*, 181–194.

Hall, D. K., Riggs, G. A., & Salomonson, V. V. (1995). Development of methods for mapping global snow cover using moderate resolution imaging spectroradiometer data. *Remote Sens. Environ.*, *54*, 127–140.

Hall, D. K., Salomonson, V. V., & Riggs, G. A. (2006). *MODIS/terra snow cover daily L3 global 0.05Deg CMG, version 5.* Boulder, Colorado USA: NASA National Snow and Ice Data Center Distributed Active Archive Center. http://dx.doi.org/10.5067/EI5HGLM2NNHN.

Hecht-Nielsen, R. (1989). Theory of the backpropagation neural network. *Neural Networks, 1989* (pp. 593–605) (IJCNN., International Joint Conference on).

Hollinger, J. P. (1991). *DMSP special sensor microwave/imager calibration/validation.* Washington, D.C.: Naval Research Laboratory.

Kelly, R. E., Chang, A. T., Tsang, L., & Foster, J. L. (2003). A prototype AMSR-E global snow area and snow depth algorithm. *Geosci. Remote Sens. IEEE Trans.*, *41*, 230–242.

Kelly, R. J., Chang, A., Foster, J., & Hall, D. (2001). Development of a passive microwave global snow monitoring algorithm for the advanced microwave scanning radiometer-EOS. *Geoscience and Remote Sensing Symposium, 2001. IGARSS '01. IEEE 2001 International* (pp. 804–806).

Klein, A. G., & Barnett, A. C. (2003). Validation of daily MODIS snow cover maps of the upper Rio Grande river basin for the 2000–2001 snow year. *Remote Sens. Environ.*, *86*, 162–176.

Koenig, L. S., & Forster, R. R. (2004). Evaluation of passive microwave snow water equivalent algorithms in the depth hoar-dominated snowpack of the Kuparuk River Watershed, Alaska, USA. *Remote Sens. Environ.*, *93*, 511–527.

Li, W., Guo, Q., & Elkan, C. (2011). Can we model the probability of presence of species without absence data? *Ecography*, *34*, 1096–1105.

Li, W., & Guo, Q. (2013). How to assess the prediction accuracy of species presence–absence models without absence data? *Ecography*, *36*, 788–799.

Li, W., & Guo, Q. (2014). A new accuracy assessment method for one-class remote sensing classification. *IEEE Trans. Geosci. Remote Sens.*, *52*, 4621–4632.

Liu, C., Berry, P. M., Dawson, T. P., & Pearson, R. G. (2005). Selecting thresholds of occurrence in the prediction of species distributions. *Ecography*, *28*, 385–393.

National Ice Center (2008). *IMS daily northern hemisphere snow and ice analysis at 1 km, 4 km, and 24 km Resolutions, Version 1.* Boulder, Colorado USA: NSIDC: National Snow and Ice Data Center. http://dx.doi.org/10.7265/N52R3PMC (updated daily).

Pulliainen, J. (2006). Mapping of snow water equivalent and snow depth in boreal and sub-arctic zones by assimilating space-borne microwave radiometer data and ground-based observations. *Remote Sens. Environ.*, *101*, 257–269.

Pulliainen, J. T., Grandell, J., & Hallikainen, M. T. (1999). HUT snow emission model and its applicability to snow water equivalent retrieval. *Geosci. Remote Sens. IEEE Trans.*, *37*, 1378–1390.

Richard, M., & Lippmann, R. (1991). Neural network classifiers estimate Bayesian a posteriori probabilities. *Neural Comput.*, *3*, 461–483.

Rijsbergen, C. J. V. (1979). *Information retrieval.* Newton, MA, USA: Butterworth Heinemann.

Romanov, P., Gutman, G., & Csiszar, I. (2000). Automated monitoring of snow cover over north America with multispectral satellite data. *J. Appl. Meteorol.*, *39*, 1866–1880.

Romanov, P., Tarpley, D., Gutman, G., & Carroll, T. (2003). Mapping and monitoring of the snow cover fraction over North America. *J. Geophys. Res. Atmos.*, *108*, 137–141.

Rosenthal, W., & Dozier, J. (1996). Automated mapping of montane snow cover at subpixel resolution from the Landsat Thematic Mapper. *Water Resour. Res.*, *32*, 115–130.

Tedesco, M., Kelly, R., Foster, J. L., & Chang, A. T. C. (2004). *AMSR-E/aqua daily L3 global snow water equivalent EASE-grids. Version 2.* Boulder, Colorado USA: NASA National Snow and Ice Data Center Distributed Active Archive Center. http://dx.doi.org/10.5067/AMSR-E/AE_DYSNO.002.

Walker, A., Derksen, C., & Goodison, B. (2005). Evaluation of passive microwave snow water equivalent retrievals across the boreal forest/tundra transition of western Canada. *Remote Sens. Environ.*, *96*, 315–327.

Walker, A. E., & Goodison, B. E. (1993). Discrimination of a wet snow cover using passive microwave satellite data. *Ann. Glaciol.*, *17*, 307–311.

Wang, X., Xie, H., Liang, T., & Huang, X. (2009). Comparison and validation of MODIS standard and new combination of Terra and Aqua snow cover products in northern Xinjiang, China. *Hydrol. Process.*, *23*, 419–429.

Yu, H., Zhang, X., Liang, T., Xie, H., Wang, X., Feng, Q., & Chen, Q. (2011). A new approach of dynamic monitoring of 5-day snow cover extent and snow depth based on MODIS and AMSR-E data from Northern Xinjiang region. *Hydrol. Process.*, *26*, 3052–3061.